Supplement of Atmos. Meas. Tech., 14, 4355–4374, 2021
https://doi.org/10.5194/amt-14-4355-2021-supplement

Atmospheric Measurement Techniques
Open Access
EGU

Supplement of

Quantifying organic matter and functional groups in particulate matter filter samples from the southeastern United States – Part 2: Spatiotemporal trends

Alexandra J. Boris et al.

Correspondence to: Ann Dillner (amdillner@ucdavis.edu)

S1 Explanations for multi-annual trends in OM

S1.1 Trends in Functional Groups

Multi-annual, regional decreases in the relative contributions of COOH and oxOCO were offset by increases in the naCO and aCOH contributions; however, in absolute terms, the concentrations of naCO and aCOH did not trend significantly (Table S1). Note that absolute and fractional trends can differ substantially: for example, although the trend in aCOH concentrations at BHM is slightly negative, the trend on a relative basis is positive (also see Fig. 3).

Table S1. Trends in concentrations (μg m^{-3} yr^{-1}) and FG/OM (%OM yr^{-1}) measured using FT-IR spectrometry. Trends were calculated using Theil–Sen regression and expressed 2011–2016 (Sect. 2.8). Confidence limits are bootstrapped at 95 % confidence. Slopes in bold are greater than the confidence limits.

Variable	Sites	Seasons	Conc. Slope ± Confidence Limit (μg m^{-3} yr^{-1})	FG/OM Slope ± Confidence Limit (%OM yr^{-1})
aCH	All	All	**-0.03** ± 0.02	-0.2 ± 0.3
aCH	CTR	All	-0.01 ± 0.03	-0.1 ± 0.4
aCH	YRK	All	-0.02 ± 0.04	0.0 ± 0.4
aCH	JST	All	-0.03 ± 0.05	-0.2 ± 0.5
aCH	BHM	All	**-0.07** ± 0.06	-0.4 ± 0.6
aCH	All	Winter	-0.02 ± 0.04	-0.1 ± 0.7
aCH	All	Spring	-0.01 ± 0.04	-0.1 ± 0.5
aCH	All	Summer	**-0.08** ± 0.06	**-0.5** ± 0.4
aCH	All	Autumn	-0.02 ± 0.05	-0.1 ± 0.6
COOH	All	All	**-0.04** ± 0.03	**-0.9** ± 0.4
COOH	CTR	All	-0.02 ± 0.04	**-0.8** ± 0.5
COOH	YRK	All	-0.04 ± 0.05	**-0.9** ± 0.8
COOH	JST	All	-0.04 ± 0.05	**-1.1** ± 0.7
COOH	BHM	All	-0.06 ± 0.06	-0.7 ± 0.9
COOH	All	Winter	-0.01 ± 0.03	0.13 ± 0.8
COOH	All	Spring	-0.04 ± 0.04	**-1.4** ± 0.7
COOH	All	Summer	**-0.12** ± 0.07	**-1.4** ± 0.6
COOH	All	Autumn	-0.02 ± 0.04	-0.5 ± 0.7
oxOCO	All	All	**-0.024** ± 0.007	**-0.59** ± 0.13

Variable	Sites	Seasons	Conc. Slope ± Confidence Limit ($\mu g\ m^{-3}\ yr^{-1}$)	FG/OM Slope ± Confidence Limit ($\%OM\ yr^{-1}$)
oxOCO	CTR	All	**-0.019** ± 0.012	**-0.71** ± 0.25
oxOCO	YRK	All	**-0.021** ± 0.014	**-0.52** ± 0.24
oxOCO	JST	All	**-0.022** ± 0.015	**-0.54** ± 0.23
oxOCO	BHM	All	**-0.037** ± 0.018	**-0.5** ± 0.3
oxOCO	All	Winter	**-0.014** ± 0.012	-0.3 ± 0.3
oxOCO	All	Spring	**-0.024** ± 0.014	**-0.82** ± 0.28
oxOCO	All	Summer	**-0.041** ± 0.017	**-0.47** ± 0.23
oxOCO	All	Autumn	**-0.021** ± 0.014	**-0.61** ± 0.20
naCO	All	All	-0.003 ± 0.008	**0.45** ± 0.21
naCO	CTR	All	0.004 ± 0.021	0.3 ± 0.4
naCO	YRK	All	0.000 ± 0.016	0.4 ± 0.4
naCO	JST	All	0.008 ± 0.017	**0.5** ± 0.3
naCO	BHM	All	-0.001 ± 0.019	0.5 ± 0.5
naCO	All	Winter	-0.014 ± 0.016	-0.3 ± 0.5
naCO	All	Spring	0.018 ± 0.019	**0.8** ± 0.4
naCO	All	Summer	0.000 ± 0.021	**0.7** ± 0.4
naCO	All	Autumn	0.009 ± 0.020	0.4 ± 0.4
aCOH	All	All	-0.009 ± 0.019	**1.16** ± 0.29
aCOH	CTR	All	0.02 ± 0.04	**1.2** ± 0.5
aCOH	YRK	All	0.00 ± 0.04	**1.0** ± 0.6
aCOH	JST	All	0.02 ± 0.04	**1.3** ± 0.5
aCOH	BHM	All	-0.01 ± 0.04	**1.0** ± 0.7
aCOH	All	Winter	0.00 ± 0.03	0.8 ± 0.8
aCOH	All	Spring	0.03 ± 0.04	**1.5** ± 0.7
aCOH	All	Summer	0.00 ± 0.05	**1.7** ± 0.6
aCOH	All	Autumn	0.01 ± 0.04	**0.7** ± 0.5

S1.2 Decline in COOH, oxOCO and aCH concentrations: Possible mechanisms

Other measurements and model results, summarized below, elucidate three probable mechanisms that link the parallel declines in oxidized OM concentrations with those in anthropogenic VOC and/or SO_2 emissions. First, photo-oxidation of anthropogenic VOCs, which accounts for ~18–30 % of OM in the SE U.S., can directly explain some portion of the decline in oxidized OM (Blanchard et al., 2013; Kim et

al., 2015; Mao et al., 2018). This anthropogenic portion is typically not discussed, with the exception of the works of Ridley et al. (2018) and Blanchard et al. (2016). Discussions have instead focused more on oxidized isoprene (biogenic) emissions, which account for ~18–36 % of OM (summer 2013; Budisulistiorini et al., 2015; Xu et al., 2015b), and introduce a second probable mechanism for OM decline. While anthropogenic emissions have themselves been declining, isoprene OM is suggested to be declining, not due to direct decrease in isoprene emissions, but indirectly due to mechanisms related to decreasing SO_2 emissions (Goldstein et al., 2009; Malm et al., 2017; Marais et al., 2017; Nguyen et al., 2014; Xu et al., 2015c). The precise mechanism for this is uncertain, but it relates to SO_4^{2-} concentrations (an oxidation product of SO_2): while some research supports a pathway related to particle acidity and/or aerosol water content (Chen et al., Submitted; Marais et al., 2017; Sareen et al., 2016; also see Sect. S1.1 discussing the possible role of aqueous oxidation), other studies suggest that isoprene OM declines are less associated with these factors (Budisulistiorini et al., 2015), and more directly associated with SO_4^{2-} concentrations and the formation of organosulfates (Schindelka et al., 2013; Xu et al., 2015c). One recent study suggests, however, that the impact of SO_4^{2-} on these observed OM concentration declines could be over-estimated (Zheng et al., 2020). Third, the oxidation pathways of anthropogenic or monoterpene VOCs may be affected by SO_4^{2-} concentration declines, with parallel pathways to the suggested decline in isoprene-derived OM. Overall, we suggest that the contribution of secondary OM, composed partially of COOH and oxOCO, is decreasing directly due to anthropogenic VOC emissions declines and/or indirectly due to SO_2 emissions declines.

S1.2.1 Decline in COOH, oxOCO and aCH concentrations: Plausibility of aqueous contribution

It is possible that the oxidation leading to this declining portion of OM occurred partially in the atmospheric aqueous phase, as hypothesized previously (Marais et al., 2015). While abundant in-cloud production of OM is not supported by model and satellite results for the SE US (Mao et al., 2018; Kim et al., 2015), wet aerosol can be an important venue for aqueous OM formation (Tan et al., 2009; McNeill, 2015), and these wet oxidation processes are likely to be regionally important (e.g., Xu et al., 2015).

S1.3 Increase in aCOH and naCO Concentrations: Possible mechanisms

A relationship of aCOH and naCO with oxidized biogenic emissions was reported in prior FT-IR spectrometry work from the SE U.S. (Liu et al., 2018a). Liu et al. demonstrated agreement with the strong aCOH and naCO contributions to OM found in other FT-IR spectrometry biogenic factors from mainly evergreen-dominated forests (Corrigan et al., 2013; Schwartz et al., 2010; Takahama et al., 2011). The seasonality of aCOH and naCO concentrations may also support a monoterpene source: slopes were steepest during the spring followed by autumn (Table S1), coincident with events driving monoterpene emissions, including bud break and needle growth in the spring and leaf fall in the autumn (Geron and Arnts, 2010; Kim, 2001). (Note that we focus here on the seasonal behavior of the less oxygenated FGs independently of the overall trend in OM by looking at changes in concentrations rather than in FG/OM.) Particular mechanisms for preferential formation of aCOH and naCO have not been suggested, but monoterpene oxidation does result in formation of these FGs (Yu et al., 1998). Less-oxidized oxygenated organic aerosol (LO-OOA; a factor identified using high resolution aerosol mass spectrometry) has also been strongly associated with monoterpenes in the SE U.S. (Xu et al., 2018; sesquiterpenes may also be related); this and other literature has identified the majority of recent SE U.S. OM as secondary products from monoterpene oxidation (Xu et al., 2015c; Zhang et al., 2018).

In concert with changes in FG distributions within OM, the concentrations of NO_x in the SEARCH network have declined (the median decreased from 0.3 ppb in 2011 to 0.2 ppb in 2016), and O_3 concentrations have increased (from a median of 31 ppb in 2011 to 34 ppb in 2016). Low-NO_x reactions, including production of additional HOM-RO_2 via autoxidation or HOM accretion, could lead to condensation of volatile aCOH and naCO-containing molecules (Pullinen et al., 2020; Pye et al., 2019; Ziemann and Atkinson, 2012). A recent lab-in-the-field study demonstrated that O_3 concentration was the only variable among many with which secondary OM mass from α-pinene oxidation was strongly correlated in ambient SE U.S. air, supporting this hypothesis (Xu et al., 2018). However, the relationship between NO_x and secondary OM production is not straight-forward: NO_x is a key reactant in O_3 and $^{\bullet}OH$ formation, and also organonitrates during the daytime, all of which contribute to OM concentrations in the SE U.S. (Pye et al., 2015; Xu et al., 2015b). A recent body of literature has worked to predict the direction of the effect of declining NO_x emissions on OM formation (summarized by Liu et al., 2018);

some of this research supports a causal relationship between NO_x concentrations and the increasing trend in aCOH and naCO fractions observed in the present work.

S1.3.1 Increase in aCOH and naCO Concentrations: Alternative Hypotheses

There are additional alternative hypotheses that may contribute to the observed trends in the contributions of aCOH and naCO to OM. O_3 increases could be responsible for enhanced OM fractions of aCOH and naCO independent of NO_x concentrations. Matching the seasonalities of the trends in aCOH and naCO concentrations (Table S1; FG/OM seasonalities are likely dominated by COOH and oxOCO), the concentrations of O_3 increased during springs and autumns 2011–2016 (while decreasing in summers). The rise in autumn O_3 concentrations has been attributed to drought conditions and meteorological patterns in the SE U.S. that are not directly linked to long-term anthropogenic NO_x declines (Zhang and Wang, 2016; -0.1 ppb yr^{-1} in SEARCH data). As stated above, aCOH and naCO can be oxidation products of monoterpenes (Liu et al., 2018a; Sax et al., 2005; Yu et al., 1999), emissions which are relatively abundant during the spring through autumn (Geron and Arnts, 2010).

As outlined by several studies of the SE U.S. (Ayres et al., 2015; Mao et al., 2018; Xu et al., 2015b; Zhang et al., 2018), organonitrates could account for a substantial fraction of OM in the region, even at low NO_x concentrations, and are known to hydrolyse efficiently to give aCOH-containing products. However, since $NO_3^{\bullet}$ concentrations would have declined alongside NO_x concentrations, it is unlikely that organonitrate hydrolysis can explain the increase in the prominence of aCOH and naCO ($NO_3^{\bullet}$ at night and NO during the day are likely responsible for SE U.S. organonitrate formation; Xu et al., 2015a). Isoprene epoxydiol (IEPOX) reactions could also generate aCOH groups in particular (Chan et al., 2010; D'Ambro et al., 2019); however, the increase in aCOH concentration is not strong in summer, which is when IEPOX chemistry is most pronounced (Budisulistiorini et al., 2016), and prior modeling work (Marais et al., 2017) and FT-IR spectrometry (e.g., Corrigan et al., 2013) work suggest that that isoprene emissions are not likely to be responsible for this growing fraction of OM.

While summertime OM in the SE U.S. includes little or no indication of biomass burning contribution (Xu et al., 2015a; Liu et al., 2018b), prescribed burning is common in the region in the spring, but also autumn and winter, and contributes substantially to OM (Zeng et al., 2008). Indicators of fires, including

total burned area in the SE U.S. and concentrations of biomass burning chemical markers, are greatest during the springs and autumns, while lowest in the summers (Larkin et al., 2014; Zhang et al., 2010). Between 2011 and 2017, the prescribed burn acreage decreased from approximately 10,297,223 to 7,576,760 acres in the SE U.S. (Coalition of Prescribed Fire Councils, 2012, 2015, 2018), and wildland acreage burned decreased, but was variable (980,000 acres in 2009 versus 720,000 acres in 2016; based on summed totals over AL, FL, GA, NC, SC, TN, and TX values published by the National Interagency Fire Center; https://www.nifc.gov/fireInfo/fireInfo_statistics.html).

FT-IR spectrometry studies have demonstrated that biomass burning can contribute naCO and aCOH material, especially when the OM is not aged for long periods of time (Takahama et al., 2013; Corrigan et al., 2013; Takahama et al., 2011; Hawkins et al., 2010). This is consistent with a source of regional smoke, although transport of smoke could be substantial, especially in the colder months when Santa Ana winds exacerbate wildfires in CA (Bytnerowicz et al., 2010). The steep spring and autumn aCOH and naCO concentration enhancements paralleled fire seasonality (Table S1) as well as O_3 concentration seasonality; these increasing O_3 concentrations could also be a result of biomass burning activities (Jaffe and Wigder, 2012), especially considering that other anthropogenic VOC emissions declined and O_3 formation potentials of some fire-emitted VOCs are substantial (Akagi et al., 2011; Derwent et al., 2007). Despite these observations, smoke was determined to be an unlikely cause of the aCOH and naCO enhancement over time based on several considerations (listed in Section 3.3.2 of the main text).

In an effort to demonstrate a causal relationship of aCOH/OM or naCO/OM to fire activities in the SE U.S., satellite observations were used to distinguish “fire” from “no fire” days in the 2011-2016 dataset (see Main Text Section 2.3). The median concentrations of prominent aerosol species, possible fire markers, and median FG/OM ratios were calculated for “fire” and “no fire” days (Figure S1).

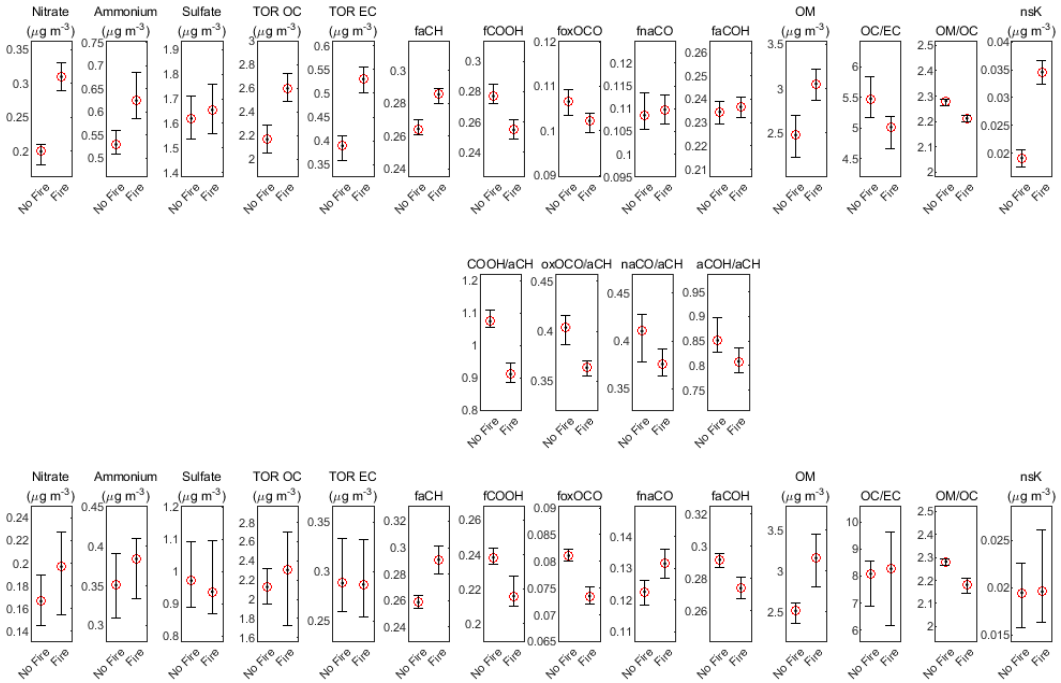

Figure S1. Box-and-whisker plots categorizing relevant concentrations and FG/OM ratios as "fire" and "no fire" days. Subplots are as follows: the top subplot is over the 2011-2016 time period and the middle subplot is FG/aCH ratios, while the bottom subplot is for only the 2016 daily dataset. FG/OM ratios are indicated as "fFG" (for example, "fCOOH"). Red circles indicate median values in each category, while bars extend to the bootstrapped 5th and 95th percent confidence limits. "nsK" is an abbreviation for non-soil potassium.

The fractions of oxOCO and COOH, with respect to OM or aCH, and for both 2011-2016 and 2016 daily datasets, were lower in "fire" samples than on "no fire" samples. The aCH/OM fraction was oppositely greater on "fire" samples than on "no fire" samples. In corroboration with the distinction of "fire" and "no fire" categories, the non-soil potassium was greater in "fire" than "no fire" samples 2011-2016. However, while the naCO/OM fraction was greater for "fire" samples in 2016 all days dataset, that trend was not observed for aCOH/OM, nor was it observed for the 2011-2016 dataset. While some work has demonstrated a difference in the aCOH/aCH and COOH/aCH in fire-impacted samples (Takahama et al., 2011; Corrigan et al., 2013), these indicative ratios were not elevated in "fire" samples in this present work. Overall, a "fingerprint" for smoke relating to aCOH and naCO was not observable, given the variation between these datasets, although the aCH/OM fraction was clearly higher in "fire" than "no fire" samples. The lack of "fingerprint" may, in part, be due to obfuscating factors such as aging of the

smoke plume, type of burn (flaming, smoldering, crop type, etc.), distance from sampling location, and the environmental conditions.

S2 OM/OC Calculation

The measured decline in FG OM concentrations between 2011 and 2016 was steeper than that observed for FG OC concentrations (Main body Section 3.1). To further contrast FG OM/OC with other estimates, OC concentration trends were compared between TOR and FT-IR measurements. A somewhat greater slope was observed in TOR OC concentrations than FT-IR spectrometry, highlighting potential causes of differences between FT-IR spectrometry estimates of OM/OC and those using TOR OC-based regression methods (Table S2; although the difference between OC measurements did not significantly vary 2011-2016, 0.04±0.04 μg m^{-3} yr^{-1} due to high method uncertainties).

S2.1 OM/OC Calculation using Regression Techniques

Two candidate multiple linear regression techniques, ordinary least squares (OLS) and error in variables (e-in-v; Simon et al., 2011), were applied for calculating OM/OC ratios with subcategories of the SEARCH functional group dataset. However, the resulting coefficients were not presented because they were often not meaningful within the understood range of possible values. In both techniques, various PM species concentrations measured in the SEARCH network (Edgerton et al., 2005) were used to calculate OM/OC ratios from a regression technique approximating the reconstructed fine mass (Simon et al., 2011; Hand et al., 2019). The methods approximate the OM/OC by assigning all $PM_{2.5}$ mass as OM in each sample if it is not attributed to other measured species (ammonium sulfate, ammonium nitrate, soil/dust, elemental carbon, and sea salt).

Although the OLS method resulted in values of OM/OC within the range of those expected overall (Turpin and Lim, 2001), other coefficients that were not within logical bounds (Simon et al., 2011). OM/OC results of the OLS regressions are summarized in Table S2, and demonstrate that values are not significantly different for any category of the data. In addition, the OM/OC values (calculated as the coefficients of TOR OC) do not match expected relationships: PM at rural sites is expected to be more aged and therefore oxidized than at urban sites; likewise, summertime PM is expected to be more oxidized

than wintertime PM. These insignificant results might be attributable to analytical measurement uncertainties of contributing network data, insufficient sample size, and/or high sampling uncertainties (Boris et al., 2019).

Table S2. Regression coefficients calculated using OLS regression from SEARCH network data components, as described by (Simon et al., 2011). Lower and upper bounds were calculated using bootstrapping.

Category	OC Coefficient (OM/OC)	Lower Bound (2.5^{th} Percentile)	Upper Bound (97.5^{th} Percentile)	Number of Samples
Urban	1.75	1.37	2.12	64
Rural	1.55	1.32	1.77	154
Winter (DJF)	1.52	1.24	1.81	57
Spring (MAM)	1.72	1.38	2.06	79
Summer (JJA)	1.45	0.79	2.11	46
Autumn (SON)	0.99	0.52	1.45	36

The e-in-v regression coefficients are not reported; values were not within logical bounds (Simon et al., 2011), confidence intervals were large in comparison to the regression coefficient values, in response to large uncertainty values inputted to the regressions. Uncertainties for each chemical species concentrations were required inputs to the e-in-v regression; these values were calculated as the root of the sum of squares of the precision of collocated samples between the Jefferson St., Atlanta, GA (JST) and collocated JST (cJST) sampling site concentrations (Boris et al., 2019; Hyslop and White, 2009), as well as the method detection limits (MDLs) reported for each relevant species by (Edgerton et al., 2005) (the average relative uncertainties for other ions was used for Cl^- since an MDL was not available). Confidence intervals about the ordinary least squares and e-in-v method OM/OC ratios were calculated using bootstrapping (n=100 with a two-tailed p=0.05). e-in-v results demonstrated that these uncertainties (MDLs and co-located sampling uncertainties) as well as the number of samples (per season, site type) were insufficient to produce meaningful results at the concentrations in the SEARCH network.

The residual between FG OC and TOR OC has not changed significantly between 2009 and 2016 (nor between 2011 and 2016, during which the trend was 0.04±0.04 μg m^{-3} yr^{-1}), and there was no seasonality in the residual (Figure S2).

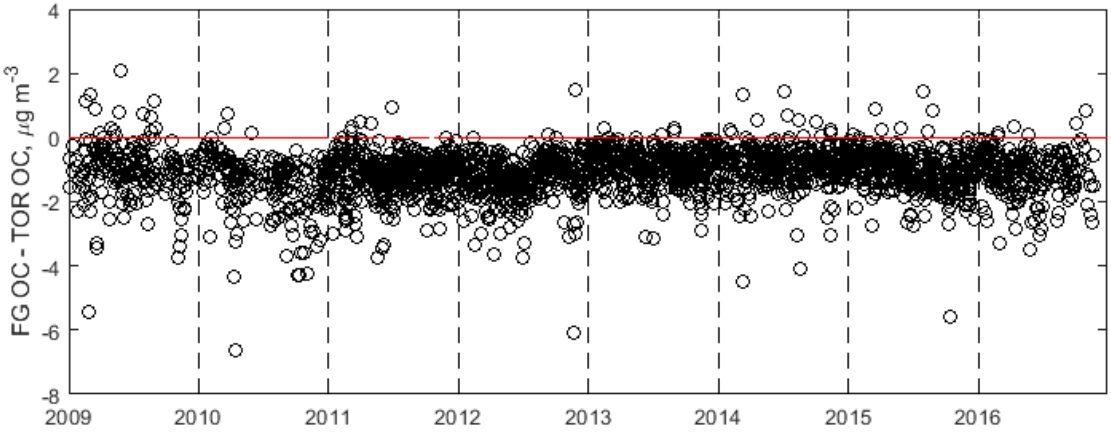

Figure S2.. Residual between concentrations of FG OC and TOR OC over the entire SEARCH 2009-2016 dataset. Dashed black lines are included at January 1st of each year, and a red line is included at a residual of 0 μg m^{-3}.

This demonstrates that the conclusions regarding long-term trend in OM would be similar with respect to OM derived from TOR OC, and furthermore that FT-IR spectrometry and TOR measurements were interchangeable over this long-term dataset. In contrast, the comparison of FT-IR spectrometry and residual OM trends demonstrated that there was an increasing difference between the two over time, with a trend of -0.08±0.07 μg m^{-3} yr^{-1} (FG OM – residual OM; Figure S3).

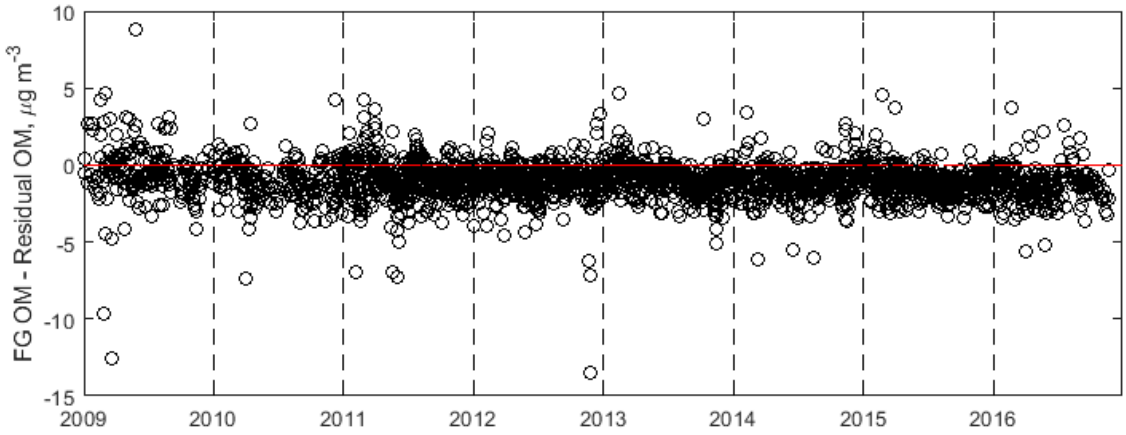

Figure S3. Residual between concentrations of FG OM and residual OM over the entire SEARCH 2009-2016 dataset. Dashed black lines are included at January 1st of each year, and a red line is included at a residual of 0 μg m^{-3}.

S3 Mean Oxidation State of Carbon

Although both describe the degree of oxidation, the OS_C and OM/OC differ in calculation. The OS_C metric up-weights the influence of O atoms (oxidation state of -2) versus H atoms (oxidation state of +1), with respect to the OM/OC (Kroll et al., 2011). While the OS_C is evaluated in terms of the contributions of the numbers of atoms, the OM/OC approximates the degree of oxidation for OM by mass. In general, the trends in OM/OC ratios and OS_C values over the 2009-2016 time period (Figure S4) were similar. The median OS_C values between -1 and +1 indicate that the sample-integrated composition of the aerosol was within the range of semi-volatile or low-volatility oxygenated OM, but more oxidized than aerosol from urban sources or biomass burning (Kroll et al., 2011). As expected, OS_C was lower (negative) for urban sites in the winter for all years than for rural sites in the summer (values were positive), although values varied between positive and negative over this time period. The overall trend in (all sites, all years) was not statistically significant (-0.001±0.003 yr^{-1}). Trends at particular sites and seasons were only significant for YRK and during winters, in which the OS_C decreased minimally (-0.008±0.005 yr^{-1} and -0.009±0.007 yr^{-1}, respectively).

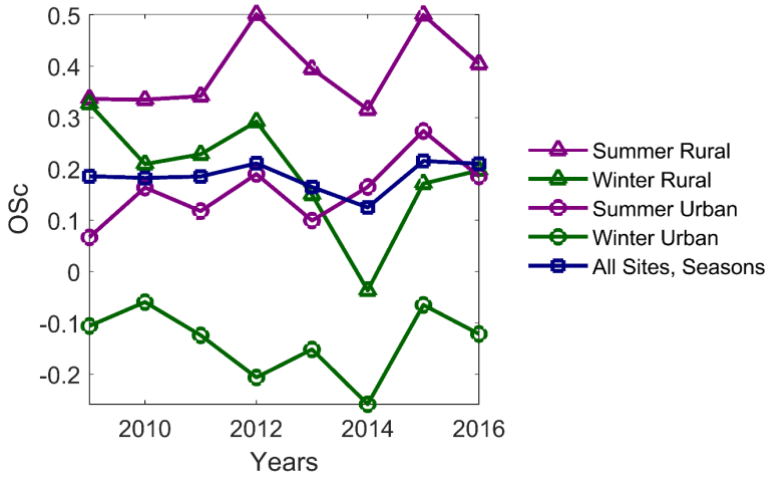

Figure S4. Trends in median carbon oxidation state (data categorized by urban/rural site category and season).

S4 Additional 2018 January and February Dataset

Additional $PM_{2.5}$ samples were collected at JST January-February 2018 at the Georgia Institute of Technology. Data are summarized in Figure S5. The 2018 January and February median organic matter composition (left subplot) represents a continuation of the declining COOH contribution to OM, alongside an increasing aCOH contribution. This is also represented by the median absolute concentrations of COOH and aCOH relative to other years (center subplot). The contribution of COOH to median OM/OC ratio (right subplot) has declined sufficiently by 2018 to apparently cause an overall decrease in median OM/OC from that in 2016.

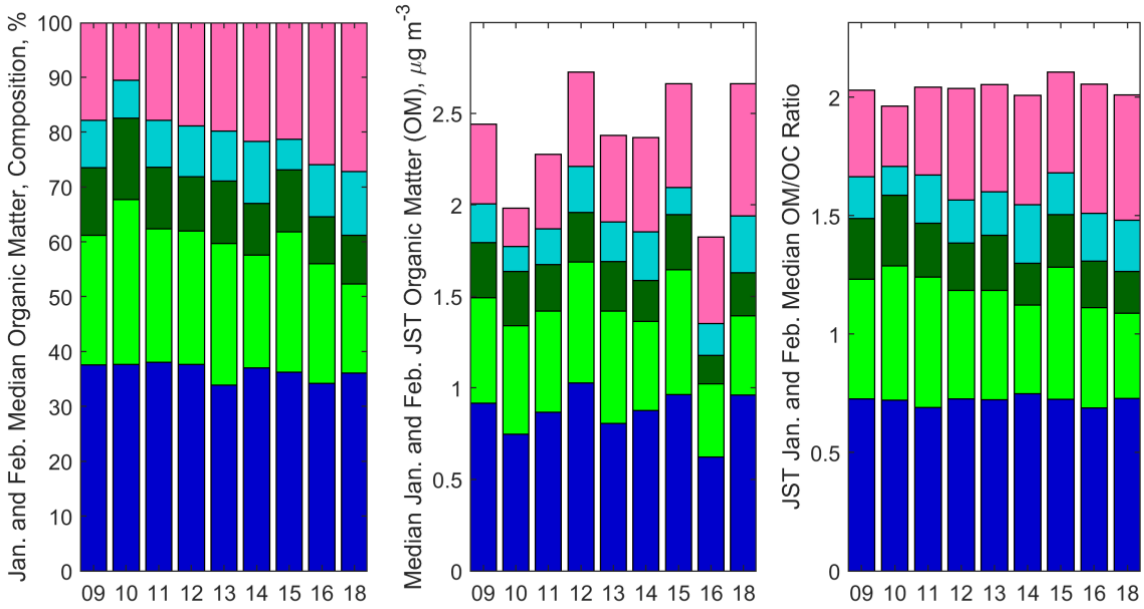

Figure S5. Medians in January and February, including 2018 extended dataset. Left: OM composition is represented as percent contribution of each functional group to total OM concentrations (see main text figures for legend). Center: absolute functional group concentrations are summed in each bar to the total OM concentration. Right: OM/OC contributions of each functional group are summed in each bar to the total OM/OC.

S5 Annual Median Sample Spectra

As discussed in the main text, FT-IR spectra of samples confirmed that the functional group composition was changing over time. This was observed in all sampling sites, with the exception of the 2008-2009 economic recession period. Baseline correction was carried out using a smoothing splines method (Kuzmiakova et al., 2016) from sample spectra between 400 and 4000 cm^{-1}. Blank spectra (including lab and field blanks; see Methods Section) were used to subtract the blank PTFE absorption and scattering (including an overlapping absorption peak at ~1790 cm^{-1}) so that the variations between median sample spectra were visible. Median spectra were calculated over the baseline corrected spectra for each year and site (Figure S6).

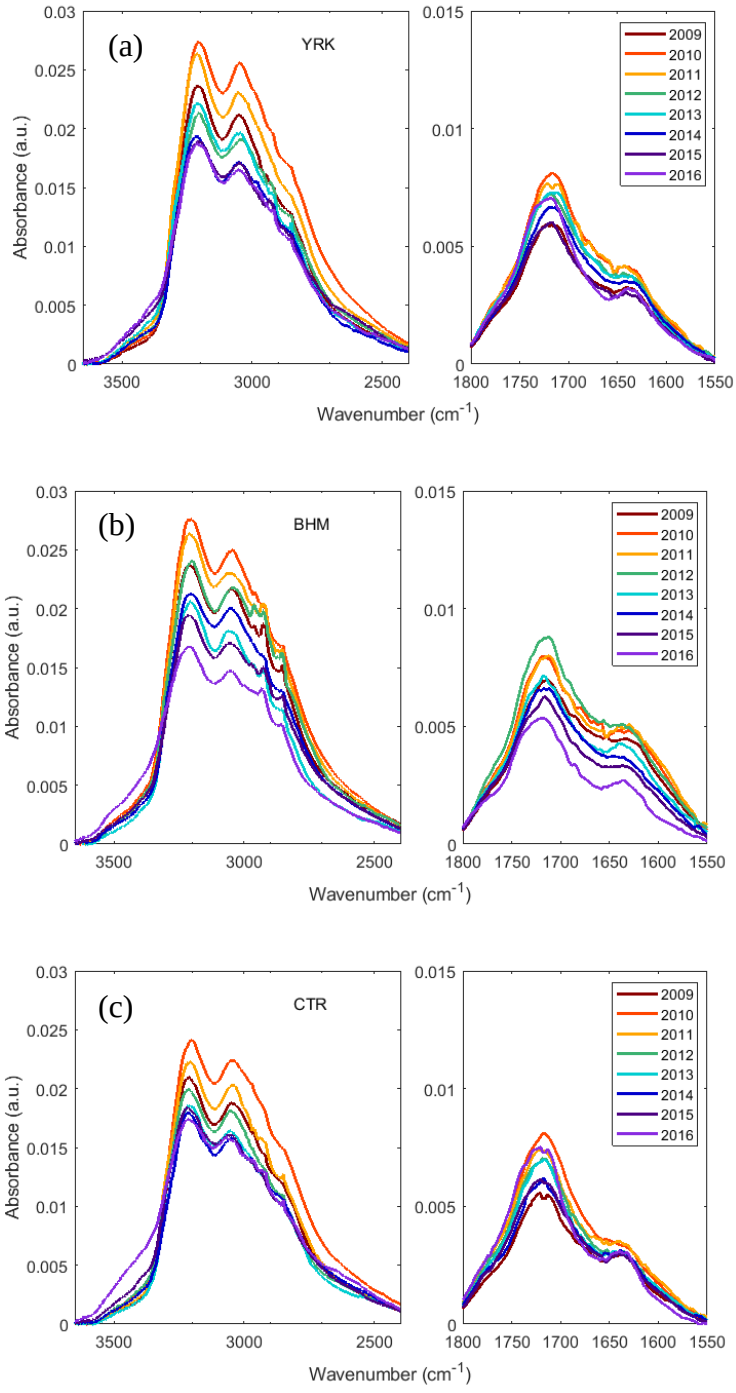

Figure S6. Annual median spectra of samples collected at each site. Colored lines, as indicated in legends, demonstrate progression of absorbance over time. Subplots show (a) YRK, (b) BHM, and (c) CTR annual median spectra. Note that peak at ~2350 cm^{-1} corresponds to Teflon filter substrate.

S6 Relationship with Wind Direction

The relationships between the wind direction (mean 24-hour direction at 10 m, measured using an RM Young 81000 sonic anemometer) and the concentrations of FT-IR OM and various other particle-phase chemical species were probed. Wind rose diagrams for each set of parameters of interested were generated using the function wind_rose function in Matlab 2016a (by M Ma; https://www.mathworks.com/matlabcentral/fileexchange/17748-wind_rose). Site and season combinations were examined to decipher whether any particular sources or meteorology might be responsible for contributions of particulate matter species (Figure S7).

It was discovered that Birmingham sources of high OM sources were variable in direction, perhaps due to regional dispersed small fires, with summer (June/July/August) high OM concentrations mainly coming from the ENE, perhaps related to emissions from a pipe foundry or coking oven (Hansen et al., 2003).

Despite Birmingham being to the NE of the Centreville site, the largest portion of springtime (March/April/May) OM originated from WNW of CTR, while the originating directions of OM during other seasons were mostly variable, with the greatest portion of samples during the autumn (September/October/November) originating from the ESE.

At Atlanta, urban sources to the SE of the site contributed to the majority of samples, but some or most higher OM samples generally originated from other directions in the winter (December/January/February). During the summer, high OM samples as well as the majority of OM in general at JST originated from the SSW, although many sources are possible from that direction.

The Yorkville site OM originated in part from Atlanta sources to the SE in the majority of samples, but higher concentrations were observed to come from areas to the west of the site, and in particular to the NW, perhaps from fires in the surrounding areas, or from industry or trees in nearby communities and rural area. During the summer, Yorkville high OM samples originated from nearly all directions, consistent with regional biogenic emissions.

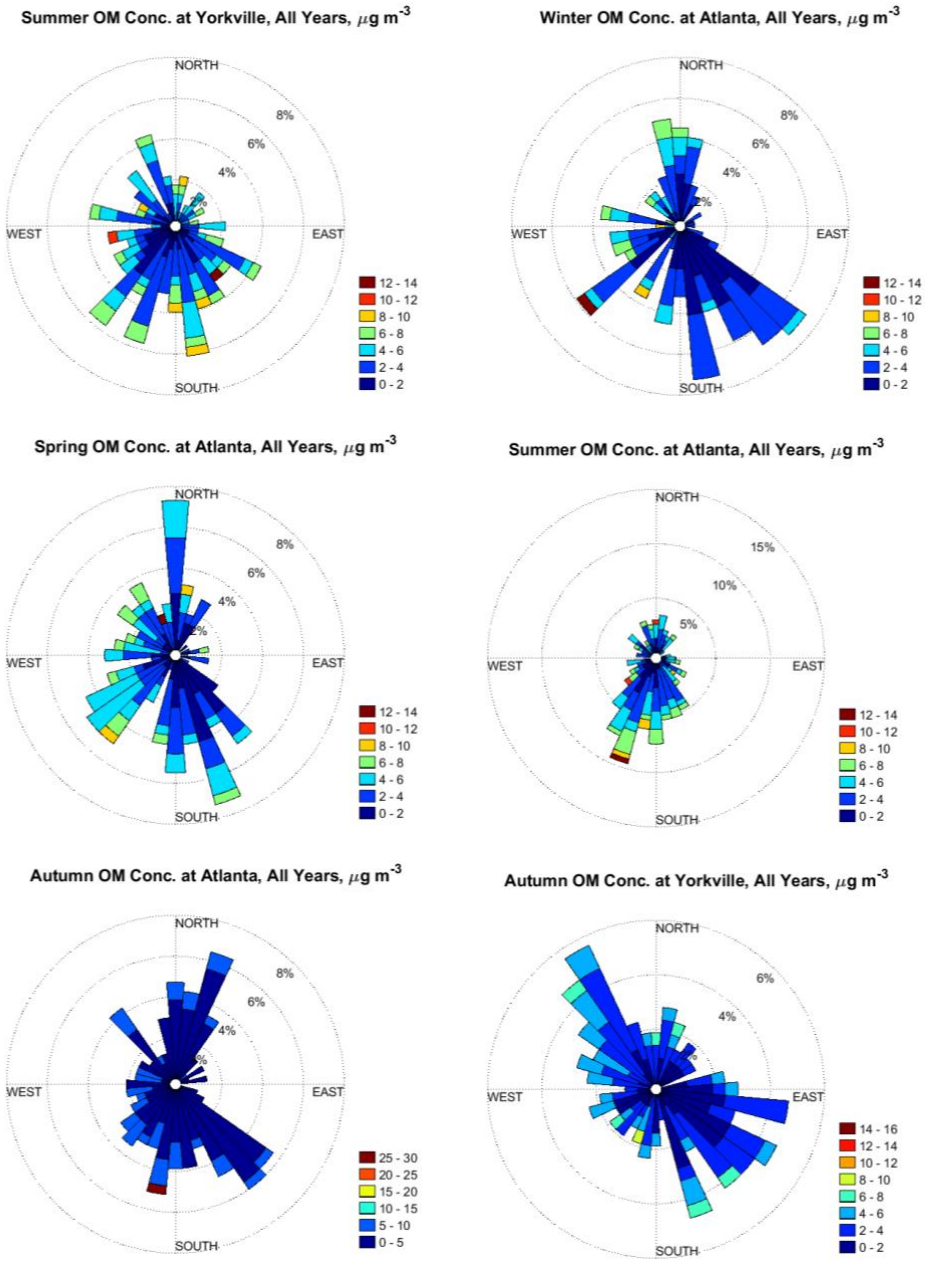

Figure S7. Wind roses for each season and site, all years.

S7 Trends in Monthly OM and Functional Groups

The monthly median OM compositions of each urban/rural site category for each site for each year 2009-2016 were plotted (Figure S8). In each case, the median absolute concentrations of OM were plotted on top of the functional group composition (right axes).

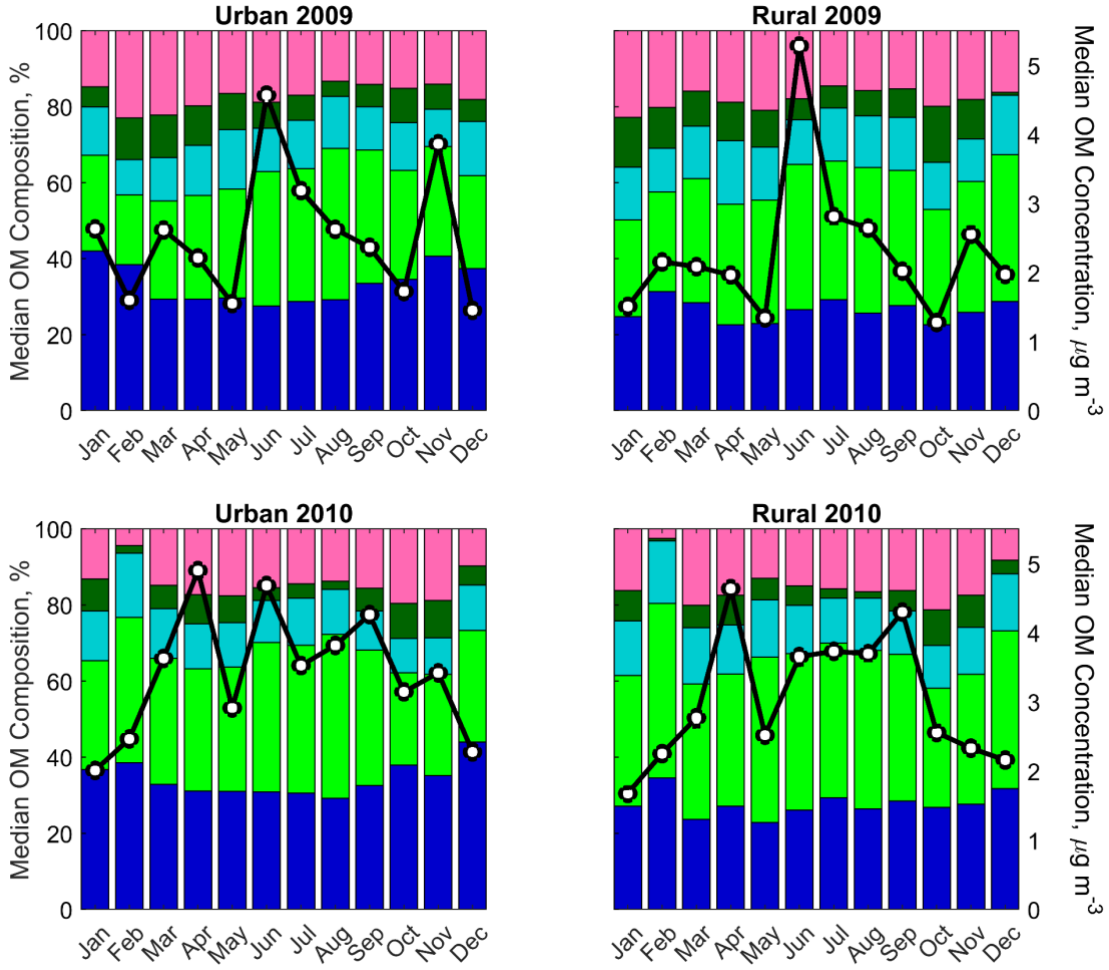

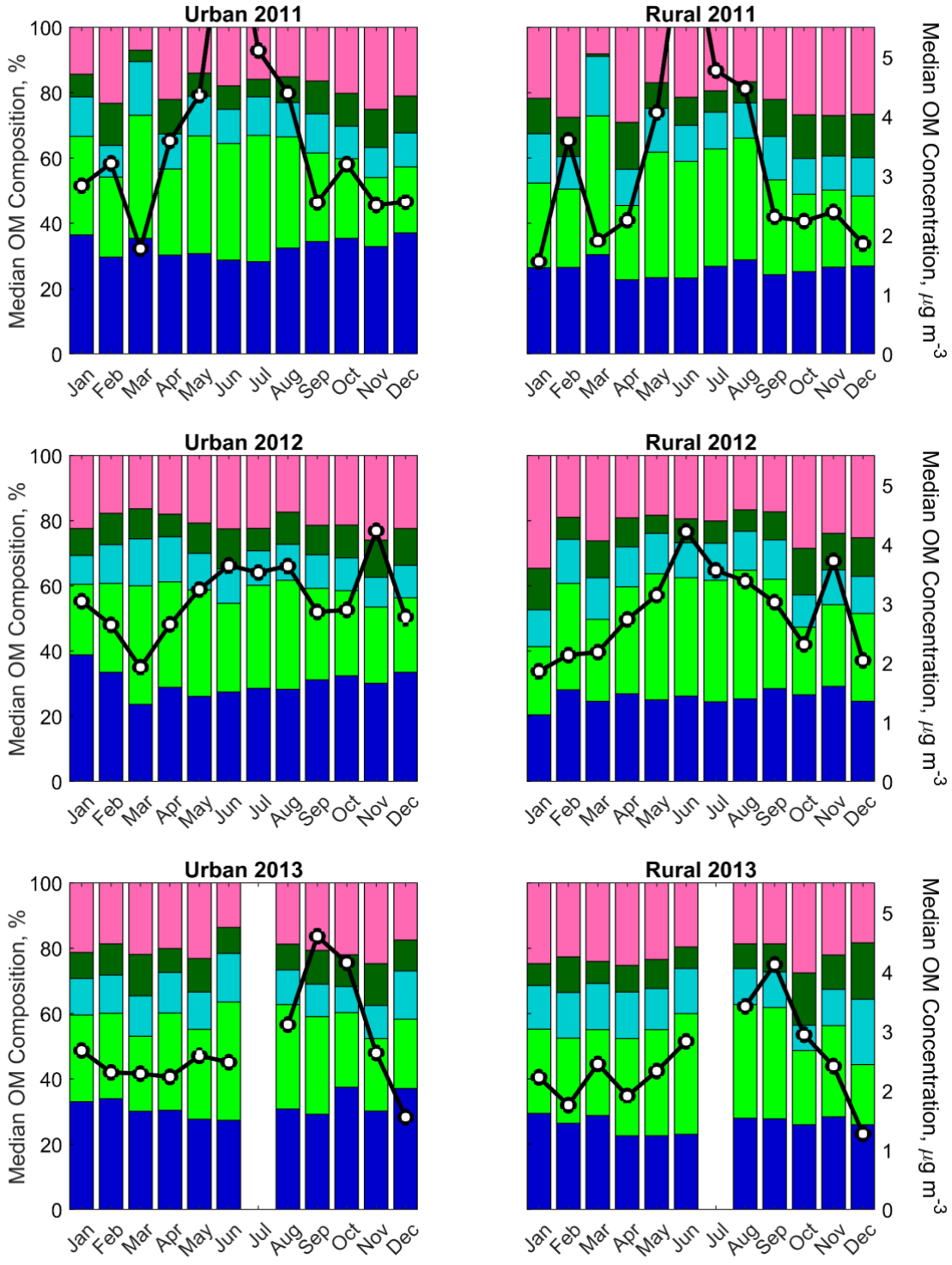
Urban 2011
Rural 2011
Urban 2012
Rural 2012
Urban 2013
Rural 2013
Median OM Composition, %
Median OM Concentration, μg m-3
0
20
40
60
80
100
0
1
2
3
4
5
Jan
Feb
Mar
Apr
May
Jun
Jul
Aug
Sep
Oct
Nov
Dec

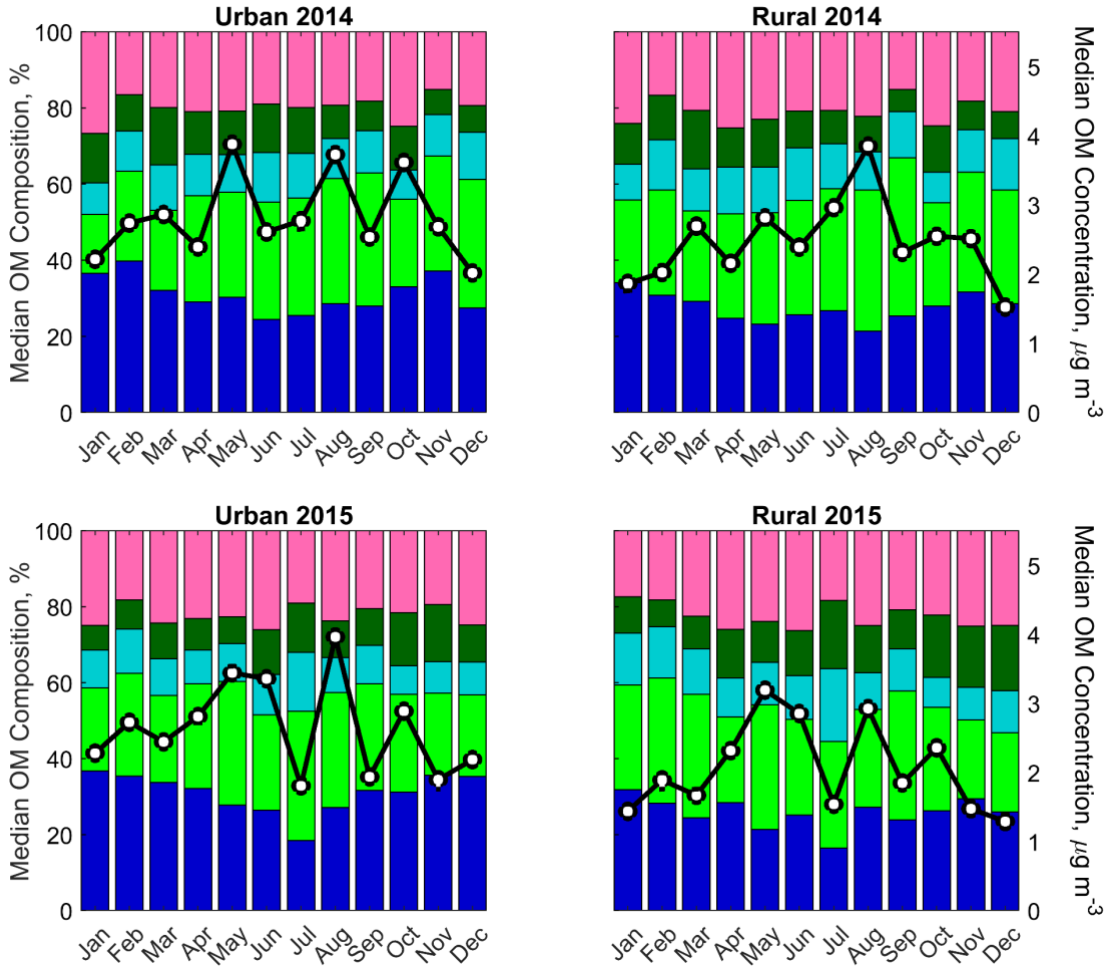
Urban 2014
Rural 2014
Urban 2015
Rural 2015
Median OM Composition, %
Median OM Concentration, μg m-3
0
20
40
60
80
100
0
1
2
3
4
5
Jan
Feb
Mar
Apr
May
Jun
Jul
Aug
Sep
Oct
Nov
Dec

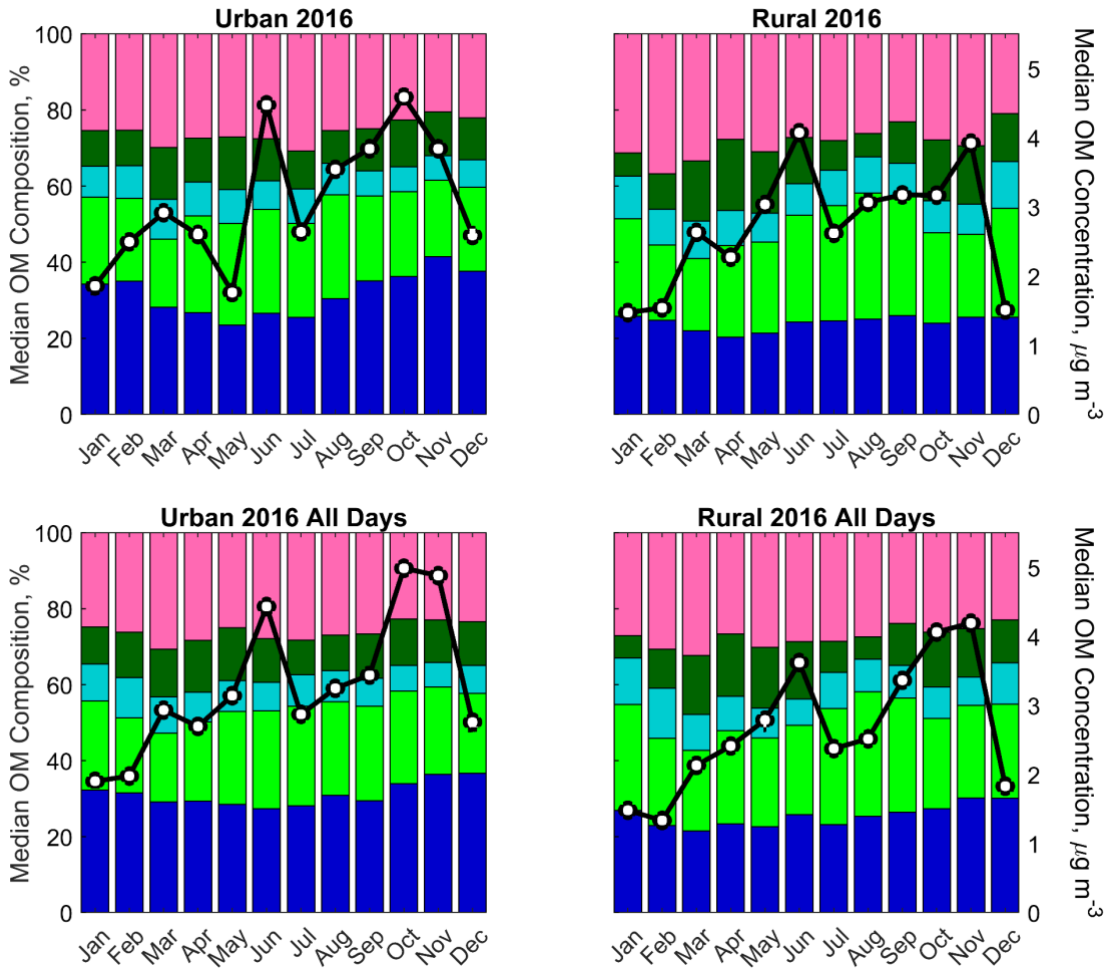

Figure S8. Monthly median OM composition and concentration, measured at. One plot is shown for each year, and for sites categorized by urban/rural location. 2016 data are demonstrated both for 1:3 day datasets and for all days.

S8 Monthly median functional group concentrations

The statistical significance of the trend in monthly concentrations of each functional group was evaluated by plotting the monthly medians and bootstrapped confidence intervals (5^{th} and 95^{th} percentiles) for each urban/rural and year grouping (Figure S9; Figure S10). These were additionally contrasted with the same plots for median *fractional* contributions of each functional group to OM concentrations. The two different perspectives on functional group quantities gave different views on the OM: while absolute concentrations of the functional groups consistently peaked in the summers, monthly patterns of the fractional contributions of the functional groups to OM varied.

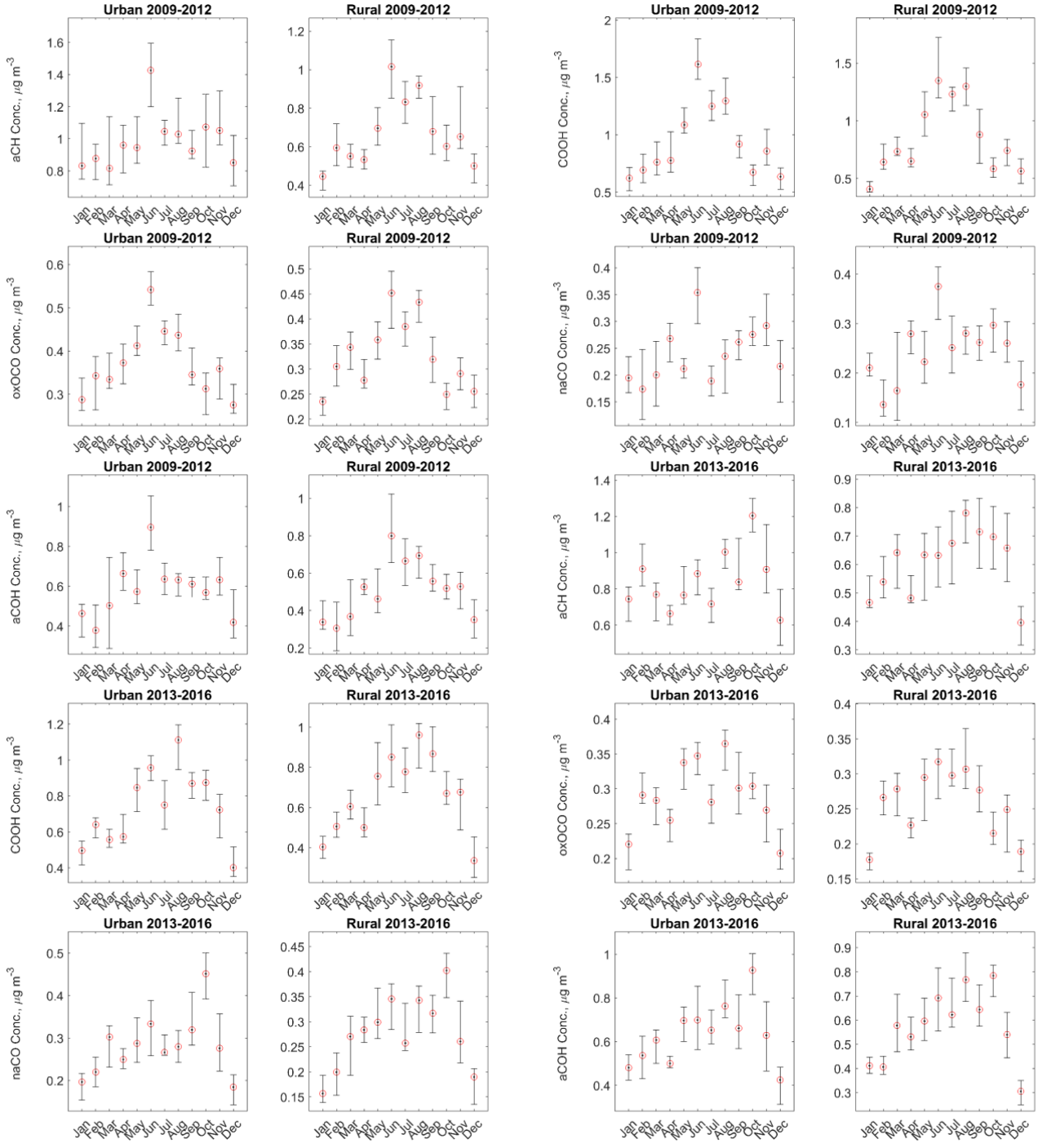

Figure S9. Monthly median concentrations of functional groups. Plots are shown for data categorized by urban/rural site location as well as subcategories of years (early = 2009-2012 and late = 2013-2016).

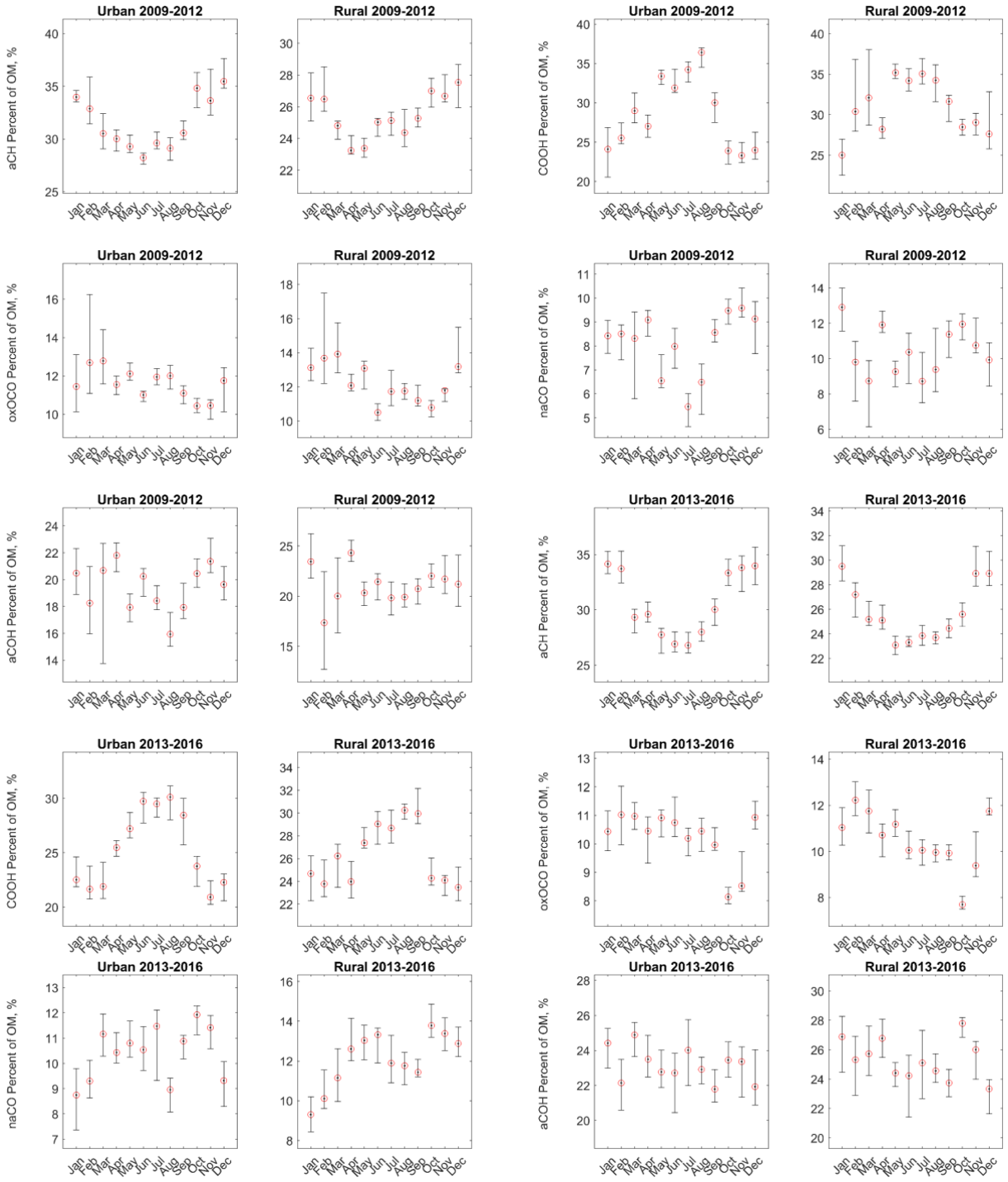

Figure S10. Monthly median contributions of functional groups to OM. Plots are shown for data categorized by urban/rural site location as well as subcategories of years (early = 2009-2012 and late = 2013-2016).

S9 Urban/Rural Ratios

Although monthly aCH concentration trends unsurprisingly mirror those of OM, the aCH monthly median urban/rural ratios were elevated compared to OM (some exceeded 1.5, especially in Alabama), indicating that the aCH was overall more attributable to urban emissions than was OM by mass. COOH trends demonstrated a distinction between the Alabama and Georgia site pairs: COOH concentrations were typically enhanced in urban Birmingham during the summer (but near one during the winter), while instead slightly enhanced in urban Atlanta during the winter. For the Alabama sites, the ratios were greater throughout the year than in the Georgia site pair, highlighting differences between the atmospheric chemical regime at the Alabama versus Georgia locations, as observed in Edgerton et al., (Edgerton et al., 2005) The monthly contrast between urban and rural site functional groups and OM (Figure S11), as well as the lack in sulfate urban/rural trends (Figure S12) overall emphasizes the importance of biogenic sources to OM in the region, but also that there is variation between chemical regimes within the region.

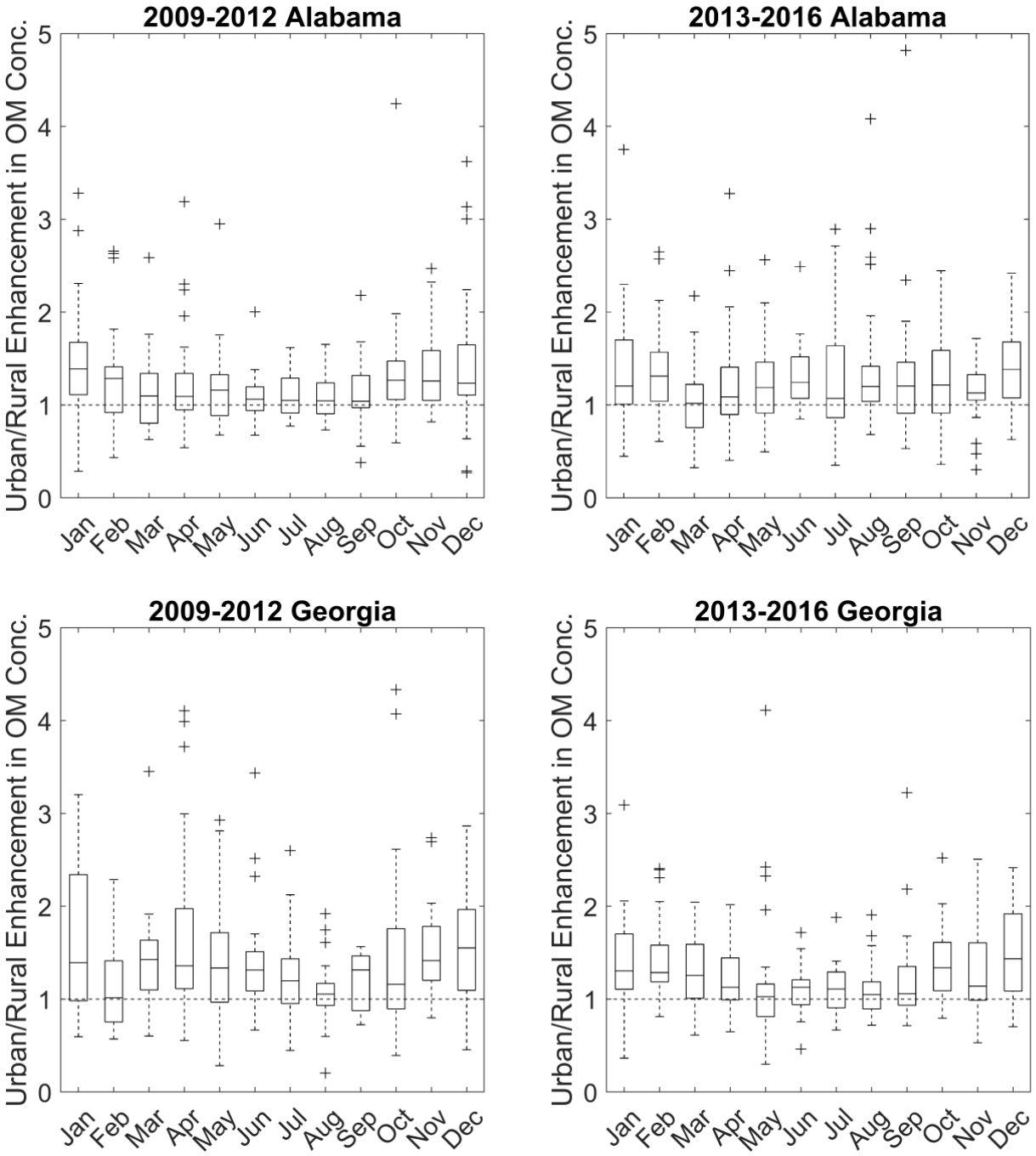

Figure S11. Monthly median urban/rural ratios of OM concentrations for Alabama (top) and Georgia (bottom) for each time period (earlier and later years).

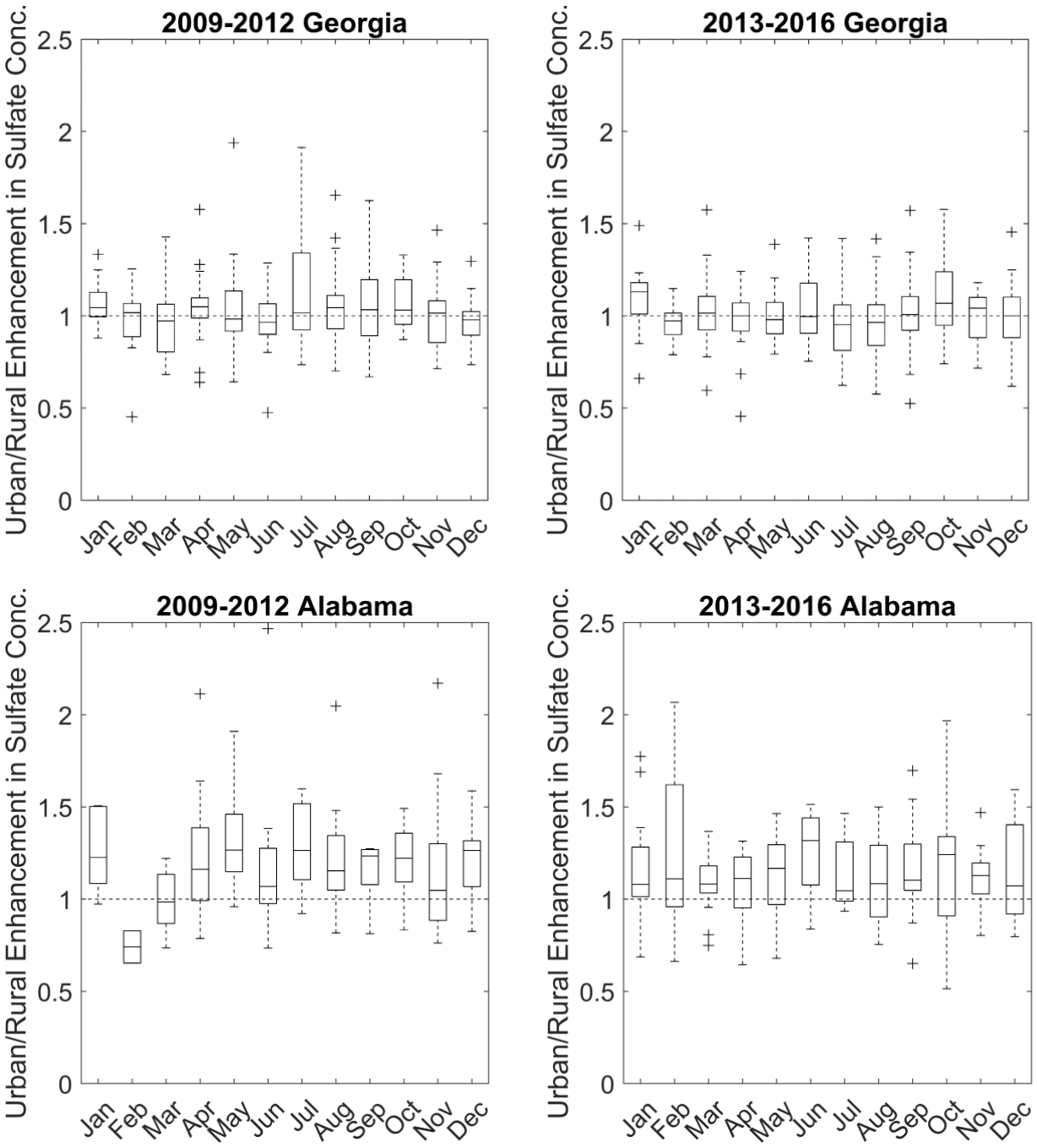

Figure S12. Monthly median urban/rural ratios of sulfate concentrations at Georgia (top) and Alabama (bottom) for each time period (earlier and later years).

5

S10 SEARCH network aerosol chemical speciation data

Chemical variables measured by the SEARCH network are summarized in the following plots of median data for each site (shown for all data 2009-2012 in Figure S13 and Figure S14, then 2013-2016 in Figure S15 and Figure S16). Seasonality as well as inter-site differences are captured by the data, including differences in the enhancement of NO_x (as well as particle NO_3^-) and elemental carbon (EC) in colder months, whereas most other variables peaked in the warmer months.

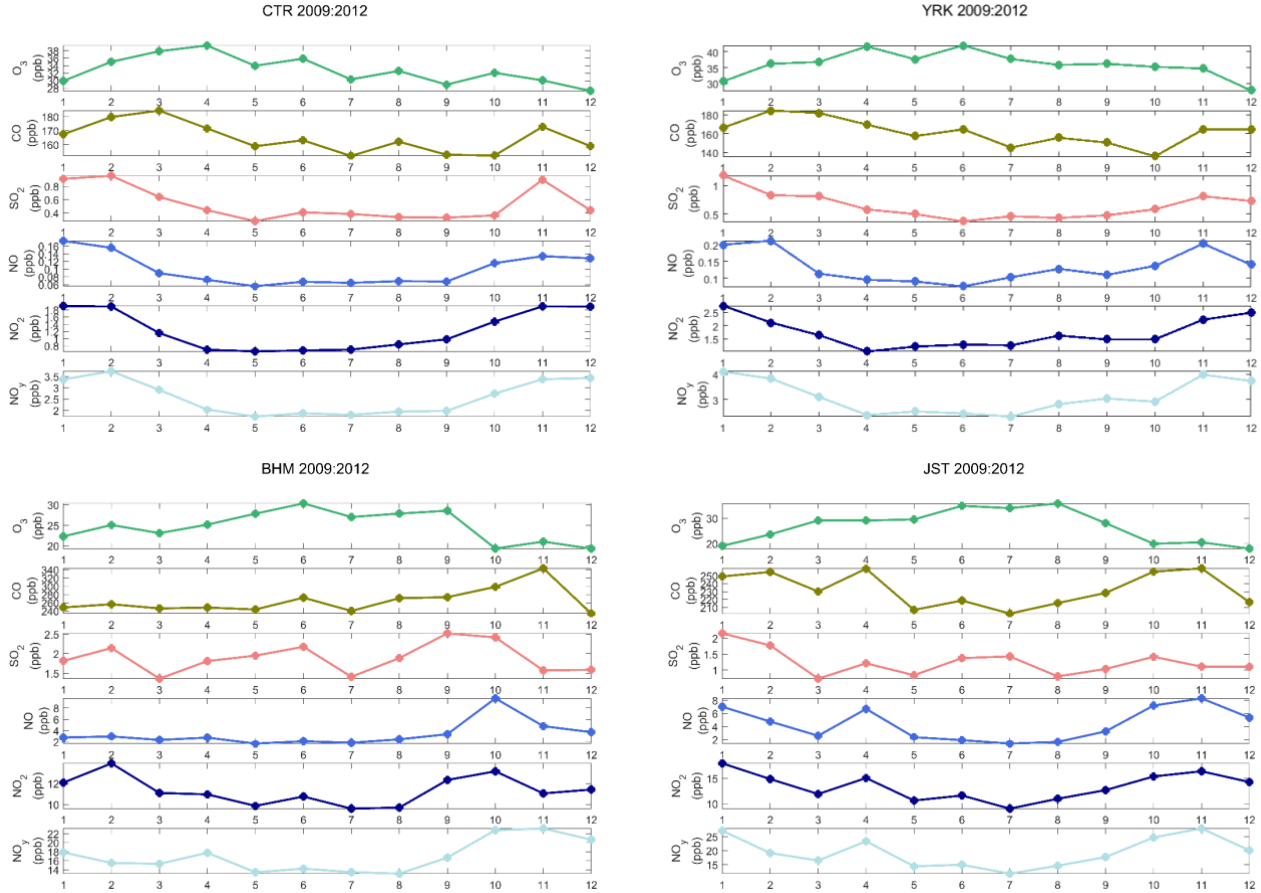

Figure S13. 2009-2012 median concentrations of SEARCH network gas particle speciation data.

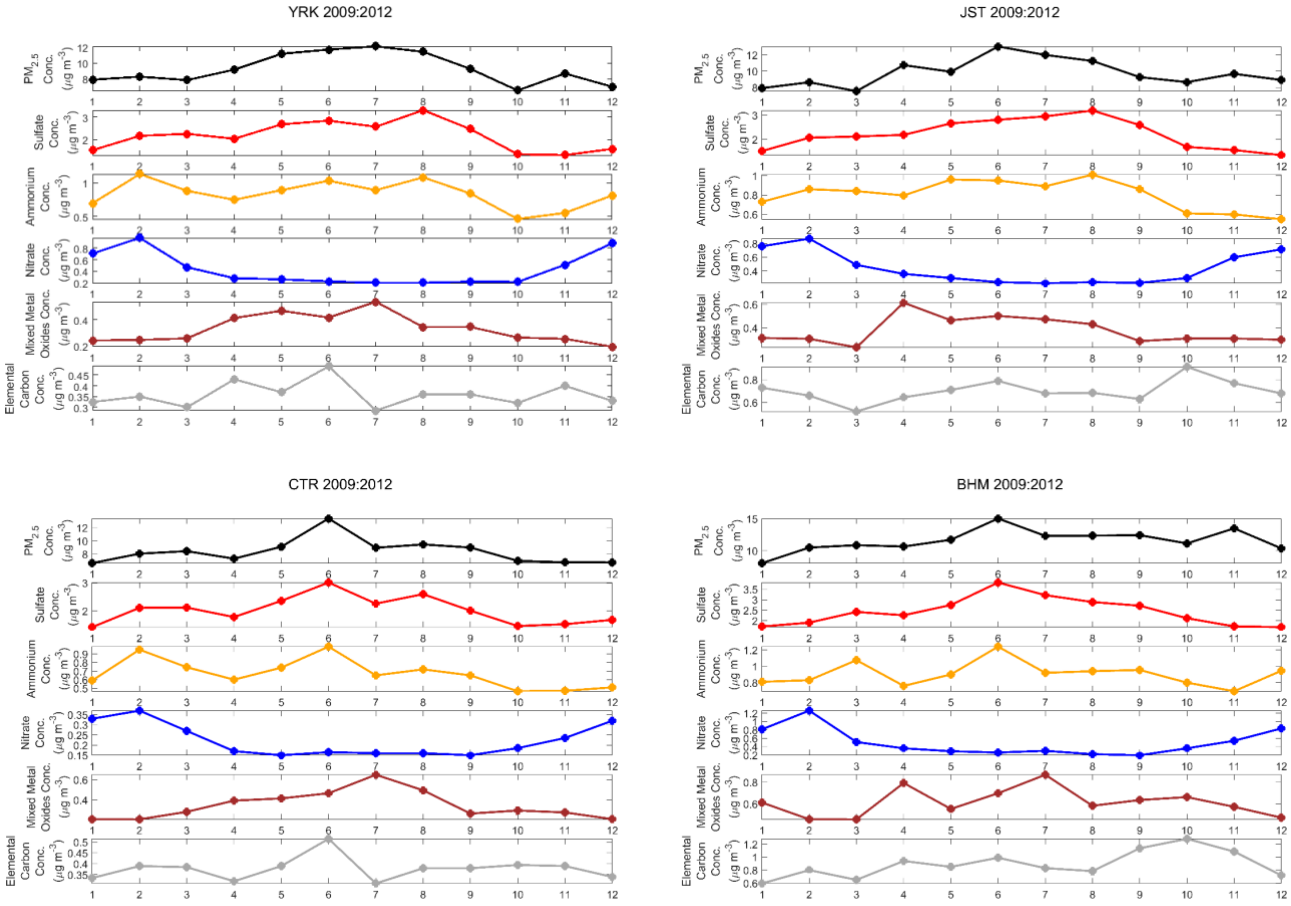

Figure S14. 2009-2012 median concentrations of SEARCH network gas particle speciation data.

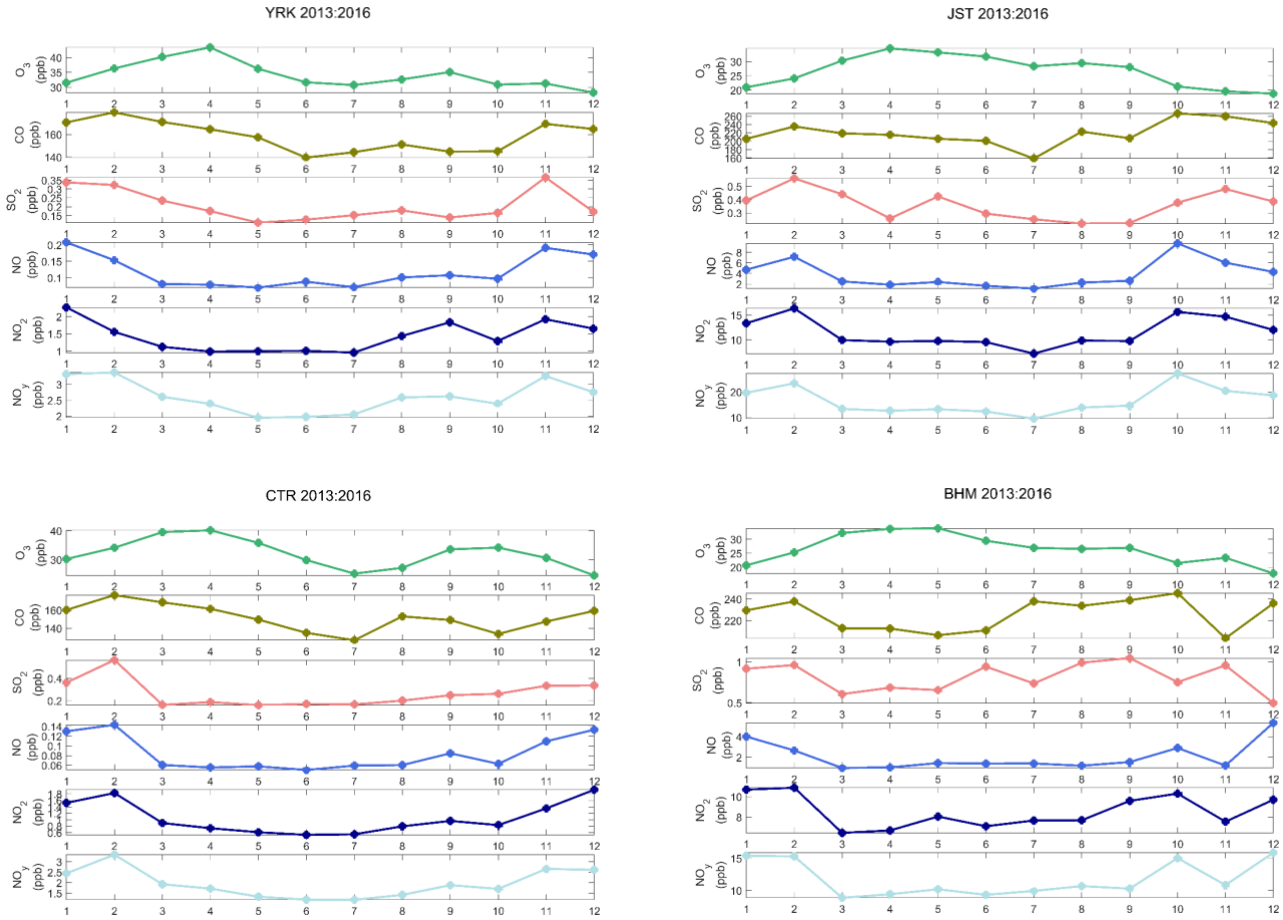

Figure S15. 2013-2016 median concentrations of SEARCH network gas speciation data.

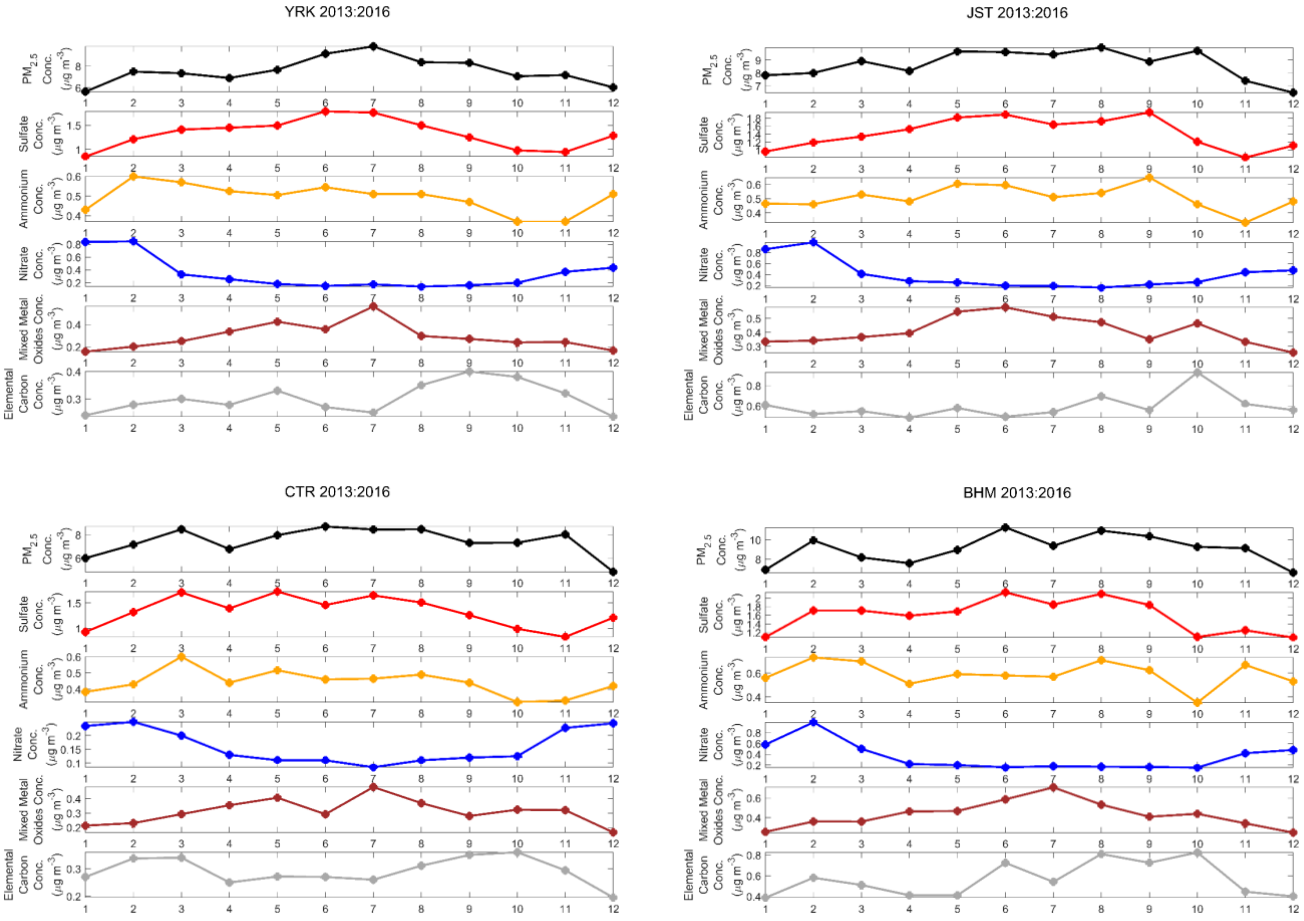

Figure S16. 2013-2016 median concentrations of SEARCH network particle speciation data.

S11 Additional 2016 Data: Alabama Sites

2016 functional group composition and OM concentrations for Alabama sites are summarized in Figure S17 (only Georgia sites were shown in the body of the paper). While similar overall seasonal observations were made for the Alabama sites, Centreville and Birmingham were perhaps more different in chemical character than were Yorkville and Atlanta. The Centreville site was expected to be more rural than the Yorkville site, and urban sources of Birmingham were distinct from those in Atlanta (Hansen et al., 2003).

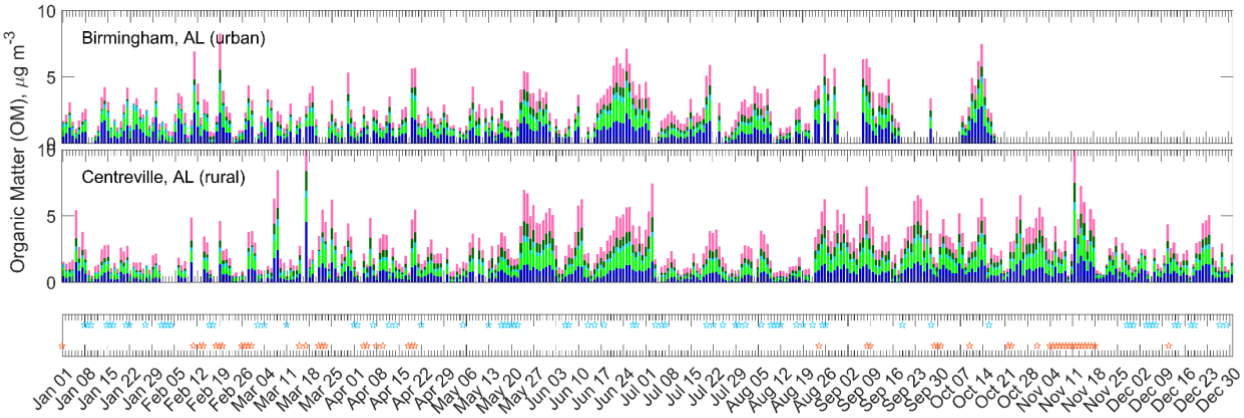

Figure S17. Organic matter concentrations, summed from the individual absolute concentrations of functional groups, are plotted for the two sites in Alabama (data for Georgia sites are shown in main paper). Precipitation and fire events are demonstrated as blue and orange markers, respectively, in the bottom subplot (from Atlanta dataset).

S12 2016 data: plots of data as normalized contributions to OM

The contributions of functional groups relative to the total OM concentrations, measured for each day in 2016 that was available and of sufficient quality (see Methods section of main paper) are plotted in Figure S18. The functional group variation during the year can be visualized more readily in this type of plot. Degree of oxidation, expressed as OM/OC and median carbon oxidation state, were also plotted.

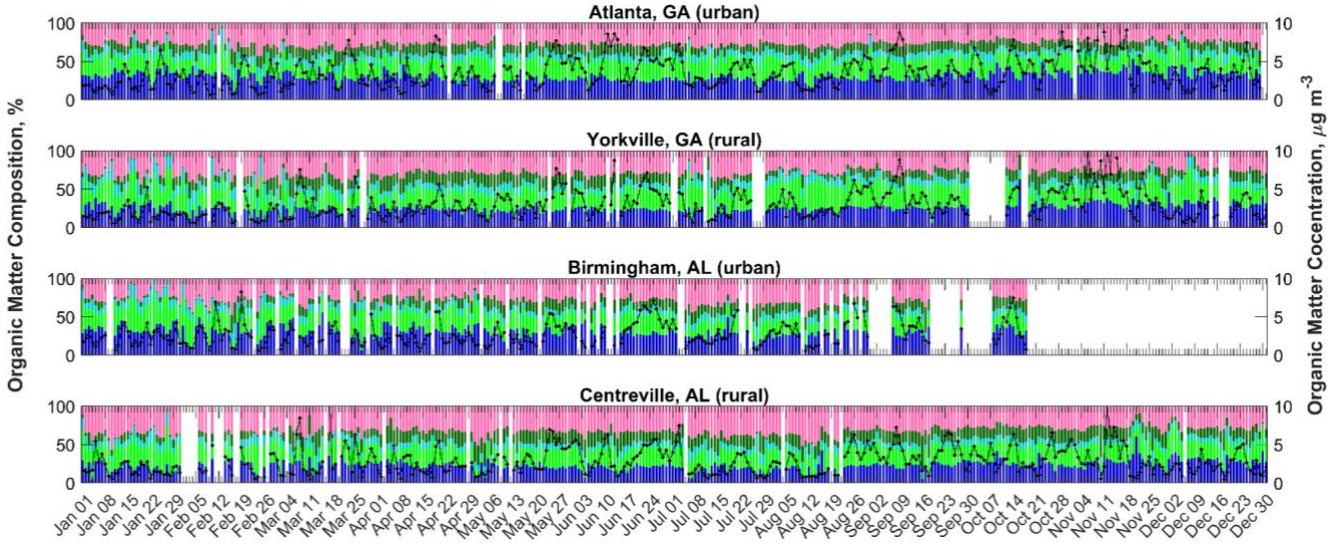

Figure S18. 2016 datasets as normalized functional group contributions to total OM concentration.

S13 Evaluation of differences between samples with and without fire impact

The median concentrations of various species within the SEARCH dataset and the FG measurements were greater in 2016 where fire was observed in the region (Figure S1c; based on positive visual identification of smoke; see Methods Section). Significantly greater values were observed (evaluated at the bootstrapped 95th percent confidence limits) for all FG concentrations and for potassium concentrations in suspected fire-impacted samples. The FG fractions of OM demonstrated differing trends, which matched the long-term trends in OM: in suspected fire-impacted samples, the aCH fraction of OM was significantly greater, the naCO and aCOH fractions of OM were not significantly different, and the COOH and oxOCO fractions of OM were significantly lower. While some of these observed differences may be caused by the seasonality of fire days, this overall suggests that the OM from aged anthropogenic and/or biogenic sources (to which was attributed declining COOH and oxOCO, but perhaps also affected a fraction of all FGs, in the multi-annual trends discussion) may be obscuring a fire fingerprint.

S14 Meteorological observations from the SEARCH network sites

Measurements of various meteorological parameters were made at the SEARCH network sites and are summarized for all days in 2016 in temporal scatter plots by site here (Figure S19, Figure S20, Figure S21, and Figure S22). The values are each 24-hour averages of the parameters, as measured by an RM Young 81000 Sonic Anemometer (wind speed and direction), ParoScientific Model 3A or 4A measurement system (temperature, RH, and barometric pressure).

As in the observations made for OM concentration and composition, more variability in meteorological parameters was observed during the shoulder and colder months, while periods of stagnation were clearly visible in data for the summer months (June, July, and August). The average RH was above 50 %, and average temperature above 20 °C for nearly all days during the summer at all sites. Even throughout the year, the average RH exceeded 30 % for most days. The average wind speed was typically lower throughout the same period, and average barometric pressure nearly constant as compared to colder months.

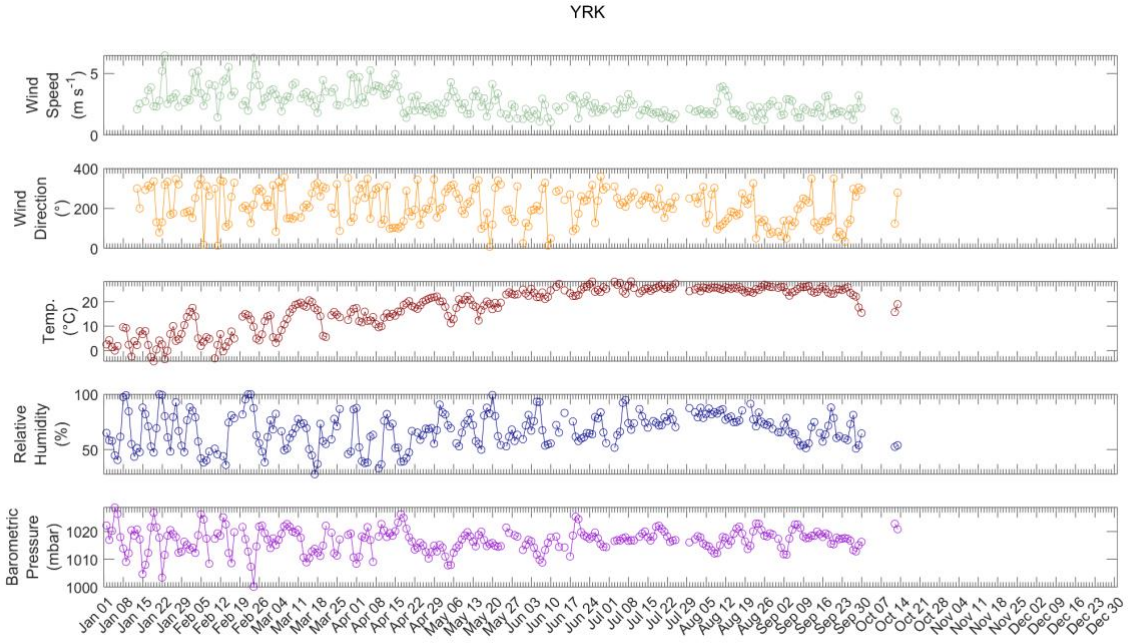

Figure S19. Meteorological parameters measured by the SEARCH network at YRK in support of the chemical speciation. Data are for all days in 2016.

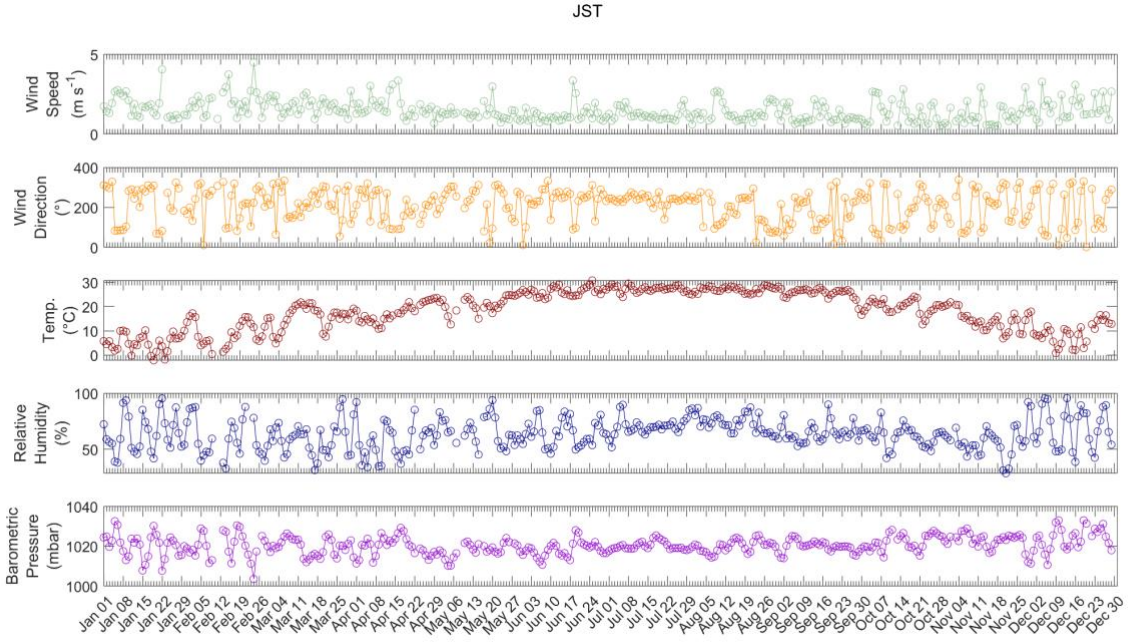

Figure S20. Meteorological parameters measured by the SEARCH network at JST in support of the chemical speciation. Data are for all days in 2016.

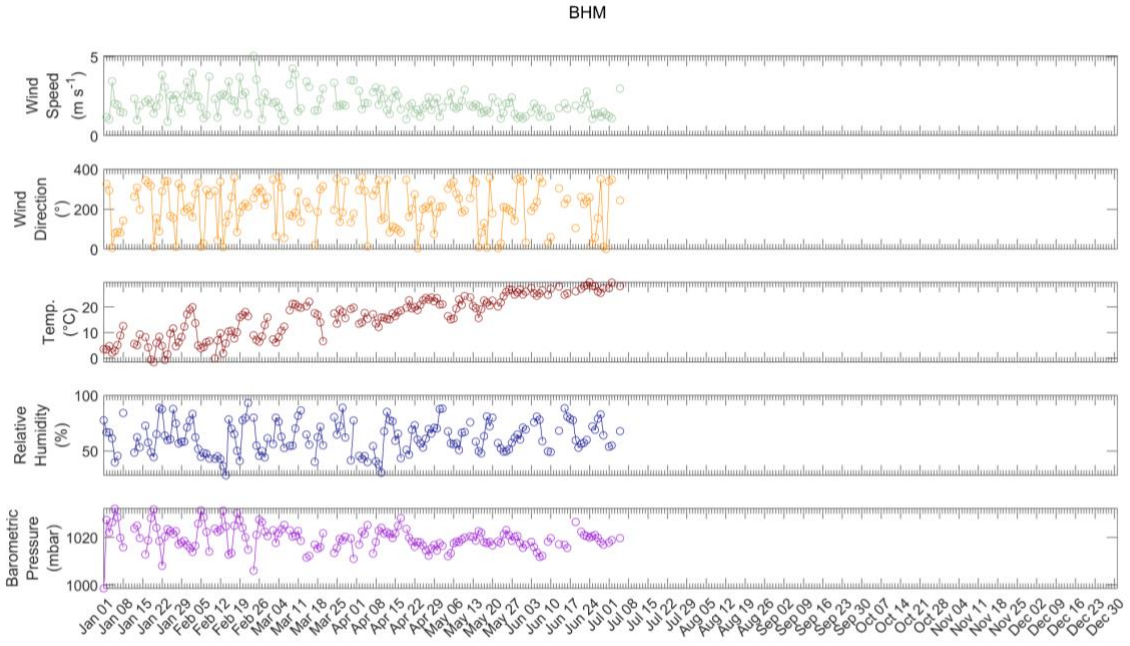

Figure S21. Meteorological parameters measured by the SEARCH network at BHM in support of the chemical speciation. Data are for all days in 2016.

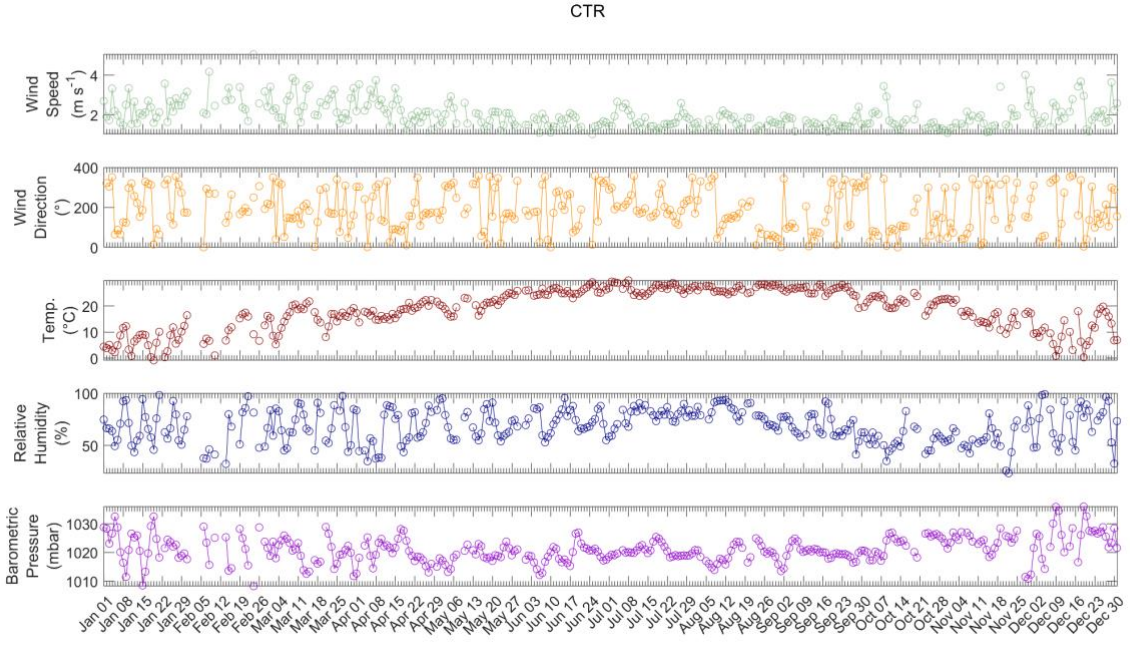

Figure S22. Meteorological parameters measured by the SEARCH network at CTR in support of the chemical speciation. Data are for all days in 2016.

S15 Weekly trends in composition: possible feedbacks of southeast U.S. aerosol on meteorology

Although a mid-week maximum in VOC concentrations has been observed previously in the SEARCH network (Blanchard et al., 2014), the median OM concentration trends observed in the present work were instead consistently lowest midweek (on Tuesdays) for 2013-2016 summers and winters at urban and rural sites (Figure S23). The same trend was observed for all FG concentrations during most seasons/sites (Table S3). The trend was less obvious during shoulder seasons (spring and autumn; not pictured for brevity) and was not observed in earlier years (2009-2012).

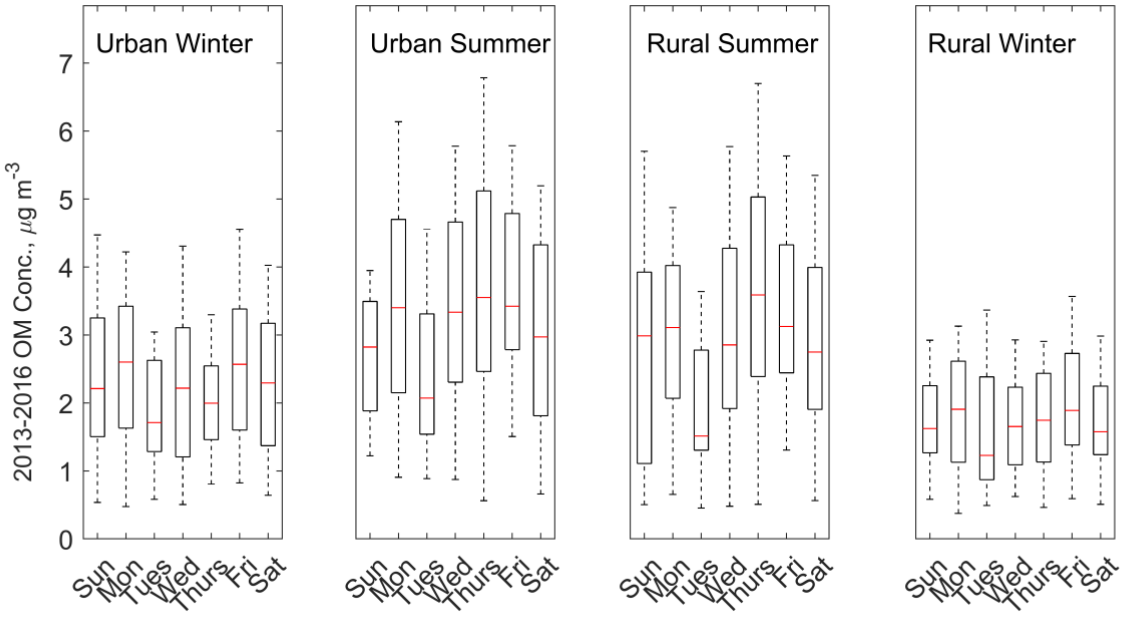

Figure S23. Median OM concentrations on each day of the week, 2013-2016, for each urban/rural and summer/winter subcategory. Whiskers extend to the 95th percent confidence limits.

These low mid-week OM concentrations in the SE U.S. coincided with high median rainfall rates (Bell et al., 2008). Bell et al. hypothesized that this greater early-week rainfall was caused by the presence of small diameter aerosol: more, smaller raindrops were formed, which delayed the formation of large droplets needed for storm invigoration. This is a well-documented phenomenon in the presence of fine aerosol, as in Andreae et al., 2004. Similarly low values on a mid-week day were observed for other chemical variables and most seasons/sites, including $PM_{2.5}$, TOR OC, TOR EC, CO, and potassium (from XRF analysis), suggesting that the trend was related to anthropogenic/combustion emissions.

Table S3. Day of week on which lowest median value was observed, for chemical and meteorological variables listed in the first column, and sample sub-categories listed in the first row. Tuesday minima are indicated in bold font. Units of each chemical/meteorological variable are listed with the variable, when relevant; "XRF" indicates that the chemical variable was measured using x-ray fluorescence spectrometry.

	Urban Winter	Urban Summer	Rural Summer	Rural Winter
OM ($\mu g\ m^{-3}$)	**Tue**	**Tue**	**Tue**	**Tue**
aCH ($\mu g\ m^{-3}$)	**Tue**	**Tue**	**Tue**	**Sun**
COOH ($\mu g\ m^{-3}$)	**Tue**	**Tue**	**Tue**	**Tue**
oxOCO ($\mu g\ m^{-3}$)	**Tue**	**Tue**	**Tue**	**Tue**
naCO ($\mu g\ m^{-3}$)	Wed	**Tue**	**Tue**	**Tue**
aCOH ($\mu g\ m^{-3}$)	**Tue**	**Tue**	**Tue**	**Tue**
aCOH/OM	Mon	Thu	Wed	Sun
COOH/OM	Sat	Sun	Sun	**Tue**
oxOCO/OM	Sat	Sun	Mon	Sat
naCO/OM	Fri	Fri	Fri	Fri
aCOH/OM	Mon	Sun	Sat	Thu
$PM_{2.5}$ ($\mu g\ m^{-3}$)	**Tue**	**Tue**	**Tue**	**Tue**
$OM/PM_{2.5}$	Thu	**Tue**	**Tue**	Thu
Sulfate ($\mu g\ m^{-3}$)	Wed	**Tue**	Sat	Wed
Nitrate ($\mu g\ m^{-3}$)	Sun	**Tue**	Sun	Sun
Sodium (XRF; $\mu g\ m^{-3}$)	Mon	Fri	Fri	Wed
Silicon (XRF; $\mu g\ m^{-3}$)	Sun	Fri	Fri	Wed
Potassium (XRF; $\mu g\ m^{-3}$)	**Tue**	**Tue**	Sat	**Tue**
Mixed Metal Oxides ($\mu g\ m^{-3}$)	Sun	Fri	Mon	Mon
TOR OC ($\mu g\ m^{-3}$)	**Tue**	**Tue**	Sun	**Tue**
TOR EC ($\mu g\ m^{-3}$)	Sun	**Tue**	**Tue**	**Tue**
Wind Speed ($m\ s^{-1}$)	Wed	Fri	Sun	Wed
Wind Direction (°)	Sat	Sun	Sun	Mon
Temperature (°C)	Fri	Fri	Mon	Thu
Relative Humidity (%)	Sat	Wed	Wed	Fri
Ozone (ppb)	Wed	Sat	**Tue**	**Tue**
CO (ppb)	Thu	**Tue**	**Tue**	**Tue**
NO (ppb)	Sun	Sun	Sun	Sun
NO_2 (ppb)	Sun	Sun	**Tue**	Sun
NO_y (ppb)	Fri	Sun	Sun	Sun

References

Akagi, S. K., Yokelson, R. J., Wiedinmyer, C., Alvarado, M. J., Reid, J. S., Karl, T., Crounse, J. D., and Wennberg, P. O.: Emission factors for open and domestic biomass burning for use in atmospheric models, 11, 4039–4072, https://doi.org/10.5194/acp-11-4039-2011, 2011.

Andreae, M. O., Rosenfeld, D., Artaxo, P., Costa, a a, Frank, G. P., Longo, K. M., and Silva-Dias, M. a F.: Smoking rain clouds over the Amazon., 303, 1337–1342, https://doi.org/10.1126/science.1092779, 2004.

Ayres, B. R., Allen, H. M., Draper, D. C., Brown, S. S., Wild, R. J., Jimenez, J. L., Day, D. a., Campuzano-Jost, P., Hu, W., de Gouw, J., Koss, A., Cohen, R. C., Duffey, K. C., Romer, P., Baumann, K., Edgerton, E., Takahama, S., Thornton, J. a., Lee, B. H., Lopez-Hilfiker, F. D., Mohr, C., Goldstein, a. H., Olson, K., and Fry, J. L.: Organic nitrate aerosol formation via NO3 + BVOC in the Southeastern US, 15, 16235–16272, https://doi.org/10.5194/acpd-15-16235-2015, 2015.

Bell, T. L., Rosenfeld, D., Kim, K. M., Yoo, J. M., Lee, M. I., and Hahnenberger, M.: Midweek increase in U.S. summer rain and storm heights suggests air pollution invigorates rainstorms, 113, 1–22, https://doi.org/10.1029/2007JD008623, 2008.

Blanchard, C. L., Tanenbaum, S., and Hidy, G. M.: Source Attribution of Air Pollutant Concentrations and Trends in the Southeastern Aerosol Research and Characterization (SEARCH) Network, Environ. Sci. Technol., 47, 13536–13545, https://doi.org/10.1021/es402876s, 2013.

Blanchard, C. L., Chow, J. C., Edgerton, E. S., Watson, J. G., Hidy, G. M., and Shaw, S.: Organic aerosols in the southeastern United States Speciated particulate carbon measurements from the SEARCH network, 2006-2010, 95, 327–333, https://doi.org/10.1016/j.atmosenv.2014.06.050, 2014.

Blanchard, C. L., Hidy, G. M., Shaw, S., Baumann, K., and Edgerton, E. S.: Effects of emission reductions on organic aerosol in the southeastern United States, Atmos. Chem. Phys., 16, 215–238, https://doi.org/10.5194/acp-16-215-2016, 2016.

Boris, A. J., Takahama, S., Weakley, A. T., Debus, B. M., Fredrickson, C. D., Esparza-Sanchez, M., Burki, C., Reggente, M., Shaw, S. L., Edgerton, E. S., and Dillner, A. M.: Quantifying organic matter and functional groups in particulate matter filter samples from the southeastern United States – Part 1: Methods, 12, 1–24, https://doi.org/10.5194/amt-12-1-2019, 2019.

Budisulistiorini, S. H., Li, X., Bairai, S. T., Renfro, J., Liu, Y., Liu, Y. J., McKinney, K. A., Martin, S. T., McNeill, V. F., Pye, H. O. T., Nenes, A., Neff, M. E., Stone, E. A., Mueller, S., Knote, C., Shaw, S. L., Zhang, Z., Gold, A., and Surratt, J. D.: Examining the effects of anthropogenic emissions on isoprene-derived secondary organic aerosol formation during the 2013 Southern Oxidant and Aerosol Study (SOAS) at the Look Rock, Tennessee ground site, Atmos. Chem. Phys., 15, 8871–8888, https://doi.org/10.5194/acp-15-8871-2015, 2015.

Budisulistiorini, S. H., Baumann, K., Edgerton, E. S., Bairai, S. T., Mueller, S., Shaw, S. L., Knipping, E. M., Gold, A., and Surratt, J. D.: Seasonal characterization of submicron aerosol chemical composition and organic aerosol sources in the southeastern United States: Atlanta, Georgia,and Look Rock, Tennessee, Atmos. Chem. Phys., 16, 5171–5189, https://doi.org/10.5194/acp-16-5171-2016, 2016.

Bytnerowicz, A., Cayan, D., Riggan, P., Schilling, S., Dawson, P., Tyree, M., Wolden, L., Tissell, R., and Preisler, H.: Analysis of the effects of combustion emissions and Santa Ana winds on ambient ozone during the October 2007 southern California wildfires, 44, 678–687, https://doi.org/10.1016/j.atmosenv.2009.11.014, 2010.

Chan, M. N. A. N. N. I. N., Surratt, J. D., Claeys, M., Edgerton, E. S., Tanner, R. L., Shaw, S. L., Zheng, M. E. I., Knipping, E. M., Eddingsaas, N. C., Wennberg, P. O., and Seinfeld, J. H.: Characterization and quantification of isoprene-derived epoxydiols in ambient aerosol in the southeastern United States., 44, 4590–6, https://doi.org/10.1021/es100596b, 2010.

Chen, Y., Guo, H., Nah, T., J., T., David, P., S., Amy, Gao, Ziqi, Vasilakos, Petros, Russell, A., Huey, L. G., Weber, R. J., and Ng, N. L.: Low-Molecular-Weight Organic Acids in the Southeastern U. S.: Formation, Partitioning, and Implications for Organic Aerosol Aging, Submitted.

Coalition of Prescribed Fire Councils: 2012 National Prescribed Fire Use Survey, 2012.

Coalition of Prescribed Fire Councils: 2015 National Prescribed Fire Use Survey, 2015.

Coalition of Prescribed Fire Councils: 2018 National Prescribed Fire Use Survey, 2018.

Corrigan, A. L., Russell, L. M., Takahama, S., Äijälä, M., Ehn, M., Junninen, H., Rinne, J., Petäjä, T., Kulmala, M., Vogel, A. L., Hoffmann, T., Ebben, C. J., Geiger, F. M., Chhabra, P., Seinfeld, J. H., Worsnop, D. R., Song, W., Auld, J., and Williams, J.: Biogenic and biomass burning organic aerosol in a boreal forest at Hyytiälä, Finland, during HUMPPA-COPEC 2010, Atmos. Chem. Phys., 13, 12233–12256, https://doi.org/10.5194/acp-13-12233-2013, 2013.

D'Ambro, E. L., Schobesberger, S., Gaston, C. J., Lopez-Hilfiker, F. D., Lee, B. H., Liu, J., Zelenyuk, A., Bell, D., Cappa, C. D., Helgestad, T., Li, Z., Guenther, A., Wang, J., Wise, M., Caylor, R., Surratt, J. D., Riedel, T., Hyttinen, N., Salo, V.-T., Hasan, G., Kurtén, T., Shilling, J. E., and Thornton, J. A.: Chamber-based insights into the factors controlling IEPOX SOA yield, composition, and volatility, 19, 11253–11265, https://doi.org/10.5194/acp-2019-271, 2019.

Derwent, R. G., Jenkin, M. E., Passant, N. R., and Pilling, M. J.: Reactivity-based strategies for photochemical ozone control in Europe, 10, 445–453, https://doi.org/10.1016/j.envsci.2007.01.005, 2007.

Edgerton, E. S., Hartsell, B. E., Saylor, R. D., Jansen, J. J., Hansen, D. A., and Hidy, G. M.: The Southeastern Aerosol Research and Characterization Study, part II: Filter-based measurements of fine

and coarse particulate matter mass and composition, 55, 1527–1542, https://doi.org/10.1080/10473289.2005.10464744, 2005.

Geron, C. D. and Arnts, R. R.: Seasonal monoterpene and sesquiterpene emissions from Pinus taeda and Pinus virginiana, 44, 4240–4251, https://doi.org/10.1016/j.atmosenv.2010.06.054, 2010.

Goldstein, A. H., Koven, C. D., Heald, C. L., and Fung, I. Y.: Biogenic carbon and anthropogenic pollutants combine to form a cooling haze over the southeastern United States, 106, 8835–8840, https://doi.org/10.1073/pnas.0904128106, 2009.

Hand, J. L., Prenni, A. J., Schichtel, B. A., Malm, W. C., and Chow, J. C.: Trends in remote PM 2.5 residual mass across the United States: Implications for aerosol mass reconstruction in the IMPROVE network, 203, 141–152, https://doi.org/10.1016/j.atmosenv.2019.01.049, 2019.

Hansen, D. A., Edgerton, E. S., Hartsell, B. E., Jansen, J. J., Kandasamy, N., Hidy, G. M., Blanchard, C. L., Hansen, D. A., Edgerton, E. S., Hartsell, B. E., Jansen, J. J., Kandasamy, N., Hidy, G. M., The, C. L. B., Hansen, D. A., Edgerton, E. S., Hartsell, B. E., Jansen, J. J., Kandasamy, N., Hidy, G. M., and Blanchard, C. L.: The Southeastern Aerosol Research and Characterization Study : Part 1 — Overview, 53, 1460–1471, https://doi.org/10.1080/10473289.2003.10466318, 2003.

Hawkins, L. N., Russell, L. M., Covert, D. S., Quinn, P. K., and Bates, T. S.: Carboxylic acids, sulfates, and organosulfates in processed continental organic aerosol over the southeast Pacific Ocean during VOCALS-REx 2008, 115, 1–16, https://doi.org/10.1029/2009JD013276, 2010.

Hyslop, N. P. and White, W. H.: Estimating precision using duplicate measurements, 59, 1032–1039, https://doi.org/10.3155/1047-3289.59.9.1032, 2009.

Jaffe, D. A. and Wigder, N. L.: Ozone production from wildfires: A critical review, 51, 1–10, https://doi.org/10.1016/j.atmosenv.2011.11.063, 2012.

Kim, J. C.: Factors controlling natural VOC emissions in a southeastern US pine forest, 35, 3279–3292, https://doi.org/10.1016/S1352-2310(00)00522-7, 2001.

Kim, P. S., Jacob, D. J., Fisher, J. A., Travis, K., Yu, K., Zhu, L., Yantosca, R. M., Sulprizio, M. P., Jimenez, J. L., Campuzano-Jost, P., Froyd, K. D., Liao, J., Hair, J. W., Fenn, M. A., Butler, C. F., Wagner, N. L., Gordon, T. D., Welti, A., Wennberg, P. O., Crounse, J. D., St. Clair, J. M., Teng, A. P., Millet, D. B., Schwarz, J. P., Markovic, M. Z., and Perring, A. E.: Sources, seasonality, and trends of southeast US aerosol: An integrated analysis of surface, aircraft, and satellite observations with the GEOS-Chem chemical transport model, 15, 10411–10433, https://doi.org/10.5194/acp-15-10411-2015, 2015.

Kroll, J. H., Donahue, N. M., Jimenez, J. L., Kessler, S. H., Canagaratna, M. R., Wilson, K. R., Altieri, K. E., Mazzoleni, L. R., Wozniak, A. S., Bluhm, H., Mysak, E. R., Smith, J. D., Kolb, C. E., and Worsnop,

D. R.: Carbon oxidation state as a metric for describing the chemistry of atmospheric organic aerosol., 3, 133–9, https://doi.org/10.1038/nchem.948, 2011.

Kuzmiakova, A., Dillner, A. M., and Takahama, S.: An automated baseline correction protocol for infrared spectra of atmospheric aerosols collected on polytetrafluoroethylene (Teflon) filters, 9, 2615–2631, https://doi.org/10.5194/amt-9-2615-2016, 2016.

Larkin, N. K., Raffuse, S. M., and Strand, T. M.: Wildland fire emissions, carbon, and climate: U.S. emissions inventories, 317, 61–69, https://doi.org/10.1016/j.foreco.2013.09.012, 2014.

Liu, J., Russell, L. M., Ruggeri, G., Takahama, S., Claflin, M. S., Ziemann, P. J., Pye, H. O. T., Murphy, B. N., Xu, L., Ng, N. L., McKinney, K. A., Budisulistiorini, S. H., Bertram, T. H., Nenes, A., and Surratt, J. D.: Regional Similarities and NO $_x$ -Related Increases in Biogenic Secondary Organic Aerosol in Summertime Southeastern United States, J. Geophys. Res. Atmos., 123, https://doi.org/10.1029/2018JD028491, 2018a.

Liu, J., Russell, L. M., Ruggeri, G., Takahama, S., Claflin, M. S., Ziemann, P. J., Pye, H. O. T., Murphy, B. N., Xu, L., Ng, N. L., McKinney, K. A., Budisulistiorini, S. H., Bertram, T. H., Nenes, A., and Surratt, J. D.: Regional Similarities and NOx-Related Increases in Biogenic Secondary Organic Aerosol in Summertime Southeastern United States, 123, 10,620-10,636, https://doi.org/10.1029/2018JD028491, 2018b.

Malm, W. C., Schichtel, B. A., Hand, J. L., and Collett, J. L.: Concurrent Temporal and Spatial Trends in Sulfate and Organic Mass Concentrations Measured in the IMPROVE Monitoring Program, 122, 10462–10476, https://doi.org/10.1002/2017JD026865, 2017.

Mao, J., Carlton, A., Cohen, R. C., Brune, W. H., Brown, S. S., Wolfe, G. M., Jimenez, J. L., Pye, H. O. T., Lee Ng, N., Xu, L., Faye McNeill, V., Tsigaridis, K., McDonald, B. C., Warneke, C., Guenther, A., Alvarado, M. J., De Gouw, J., Mickley, L. J., Leibensperger, E. M., Mathur, R., Nolte, C. G., Portmann, R. W., Unger, N., Tosca, M., and Horowitz, L. W.: Southeast Atmosphere Studies: Learning from model-observation syntheses, 18, 2615–2651, https://doi.org/10.5194/acp-18-2615-2018, 2018.

Marais, E. A., Jacob, D. J., Jimenez, J. L., Campuzano-Jost, P., Day, D. A., Hu, W., Krechmer, J., Zhu, L., Kim, P. S., Miller, C. C., Fisher, J. A., Travis, K., Yu, K., Hanisco, T. F., Wolfe, G. M., Arkinson, H. L., Pye, H. O. T., Froyd, K. D., Liao, J., and McNeill, V. F.: Aqueous-phase mechanism for secondary organic aerosol formation from isoprene: Application to the Southeast United States and co-benefit of SO2 emission controls, 15, 32005–32047, https://doi.org/10.5194/acpd-15-32005-2015, 2015.

Marais, E. A., Jacob, D. J., Turner, J. R., and Mickley, L. J.: Evidence of 1991–2013 decrease of biogenic secondary organic aerosol in response to SO $_2$ emission controls, Environ. Res. Lett., 12, 054018, https://doi.org/10.1088/1748-9326/aa69c8, 2017.

McNeill, V. F.: Aqueous organic chemistry in the atmosphere: Sources and chemical processing of organic aerosols, 49, 1237–1244, https://doi.org/10.1021/es5043707, 2015.

Nguyen, T. B., Coggon, M. M., Bates, K. H., Zhang, X., Schwantes, R. H., Schilling, K. A., Loza, C. L., Flagan, R. C., Wennberg, P. O., and Seinfeld, J. H.: Organic aerosol formation from the reactive uptake of isoprene epoxydiols (IEPOX) onto non-acidified inorganic seeds, 14, 3497–3510, https://doi.org/10.5194/acp-14-3497-2014, 2014.

Pullinen, I., Schmitt, S., Kang, S., Sarrafzadeh, M., Schlag, P., Andres, S., Kleist, E., Mentel, T. F., Rohrer, F., Springer, M., Tillmann, R., Wildt, J., Wu, C., Zhao, D., Wahner, A., and Kiendler-Scharr, A.: Impact of NOx on secondary organic aerosol (SOA) formation from α-pinene and β-pinene photooxidation: the role of highly oxygenated organic nitrates, Atmos. Chem. Phys., 20, 10125–10147, https://doi.org/10.5194/acp-20-10125-2020, 2020.

Pye, H. O. T., Luecken, D. J., Xu, L., Boyd, C. M., Ng, N. L., Baker, K. R., Ayres, B. R., Bash, J. O., Baumann, K., Carter, W. P. L., Edgerton, E., Fry, J. L., Hutzell, W. T., Schwede, D. B., and Shepson, P. B.: Modeling the Current and Future Roles of Particulate Organic Nitrates in the Southeastern United States, Environ. Sci. Technol., 49, 14195–14203, https://doi.org/10.1021/acs.est.5b03738, 2015.

Pye, H. O. T., D'Ambro, E. L., Lee, B. H., Schobesberger, S., Takeuchi, M., Zhao, Y., Lopez-Hilfiker, F., Liu, J., Shilling, J. E., Xing, J., Mathur, R., Middlebrook, A. M., Liao, J., Welti, A., Graus, M., Warneke, C., de Gouw, J. A., Holloway, J. S., Ryerson, T. B., Pollack, I. B., and Thornton, J. A.: Anthropogenic enhancements to production of highly oxygenated molecules from autoxidation, 116, 6641–6646, https://doi.org/10.1073/pnas.1810774116, 2019.

Ridley, D. A., Heald, C. L., Ridley, K. J., and Kroll, J. H.: Causes and consequences of decreasing atmospheric organic aerosol in the United States, Proc Natl Acad Sci USA, 115, 290–295, https://doi.org/10.1073/pnas.1700387115, 2018.

Sareen, N., Carlton, A. G., Surratt, J. D., Gold, A., Lee, B., Lopez-Hilfiker, F. D., Mohr, C., Thornton, J. A., Zhang, Z., Lim, Y. B., and Turpin, B. J.: Identifying precursors and aqueous organic aerosol formation pathways during the SOAS campaign, 1–42, https://doi.org/10.5194/acp-2016-200, 2016.

Sax, M., Zenobi, R., Baltensperger, U., and Kalberer, M.: Time Resolved Infrared Spectroscopic Analysis of Aerosol Formed by Photo-Oxidation of 1,3,5-Trimethylbenzene and α-Pinene, Aerosol Science and Technology, 39, 822–830, https://doi.org/10.1080/02786820500257859, 2005.

Schindelka, J., Iinuma, Y., Hoffmann, D., and Herrmann, H.: Sulfate radical-initiated formation of isoprene-derived organosulfates in atmospheric aerosols, 165, 237–259, https://doi.org/10.1039/c3fd00042g, 2013.

Schwartz, R. E., Russell, L. M., Sjostedt, S. J., Vlasenko, A., Slowik, J. G., Abbatt, J. P. D., MacDonald, A. M., Li, S. M., Liggio, J., Toom-Sauntry, D., and Leaitch, W. R.: Biogenic oxidized organic functional

groups in aerosol particles from a mountain forest site and their similarities to laboratory chamber products, 10, 5075–5088, https://doi.org/10.5194/acp-10-5075-2010, 2010.

Simon, H., Bhave, P. V, Swall, J. L., Frank, N. H., and Malm, W. C.: Determining the spatial and seasonal variability in OM/OC ratios across the US using multiple regression, 11, 2933–2949, https://doi.org/10.5194/acp-11-2933-2011, 2011.

Takahama, S., Schwartz, R. E., Russell, L. M., MacDonald, A. M., Sharma, S., and Leaitch, W. R.: Organic functional groups in aerosol particles from burning and non-burning forest emissions at a high-elevation mountain site, 11, 6367–6386, https://doi.org/10.5194/acp-11-6367-2011, 2011.

Takahama, S., Johnson, A., Guzman Morales, J., Russell, L. M., Duran, R., Rodriguez, G., Zheng, J., Zhang, R., Toom-Sauntry, D., and Leaitch, W. R.: Submicron organic aerosol in Tijuana, Mexico, from local and Southern California sources during the Calmex campaign, 70, 500–512, https://doi.org/10.1016/j.atmosenv.2012.07.057, 2013.

Tan, Y., Perri, M. J., Seitzinger, S. P., and Turpin, B. J.: Effects of Precursor Concentration and Acidic Sulfate in Aqueous Glyoxal-OH Radical Oxidation and Implications for Secondary Organic Aerosol, 43, 8105–8112, 2009.

Turpin, B. J. and Lim, H.-J.: Species Contributions to PM2.5 Mass Concentrations: Revisiting Common Assumptions for Estimating Organic Mass, 35, 602–610, https://doi.org/10.1080/02786820152051454, 2001.

Xu, L., Suresh, S., Guo, H., Weber, R. J., and Ng, N. L.: Aerosol characterization over the southeastern United States using high resolution aerosol mass spectrometry: spatial and seasonal variation of aerosol composition, sources, and organic nitrates, 15, 10479–10552, https://doi.org/10.5194/acp-15-7307-2015, 2015a.

Xu, L., Suresh, S., Guo, H., Weber, R. J., and Ng, N. L.: Aerosol characterization over the southeastern United States using high-resolution aerosol mass spectrometry: spatial and seasonal variation of aerosol composition and sources with a focus on organic nitrates, Atmos. Chem. Phys., 15, 7307–7336, https://doi.org/10.5194/acp-15-7307-2015, 2015b.

Xu, L., Guo, H., Boyd, C. M., Klein, M., Bougiatioti, A., Cerully, K. M., Hite, J. R., Isaacman-VanWertz, G., Kreisberg, N. M., Knote, C., Olson, K., Koss, A., Goldstein, A. H., Hering, S. V., de Gouw, J., Baumann, K., Lee, S.-H., Nenes, A., Weber, R. J., and Ng, N. L.: Effects of anthropogenic emissions on aerosol formation from isoprene and monoterpenes in the southeastern United States, Proc Natl Acad Sci USA, 112, 37–42, https://doi.org/10.1073/pnas.1417609112, 2015c.

Xu, L., Pye, H. O. T., He, J., Chen, Y., Murphy, B. N., and Ng, N. L.: Experimental and model estimates of the contributions from biogenic monoterpenes and sesquiterpenes to secondary organic aerosol in the

southeastern United States, Atmos. Chem. Phys., 18, 12613–12637, https://doi.org/10.5194/acp-18-12613-2018, 2018.

Yu, J., Flagan, R. C., and Seinfeld, J. H.: Identification of Products Containing −COOH, −OH, and −CO in Atmospheric Oxidation of Hydrocarbons, 32, 2357–2370, https://doi.org/10.1021/es980129x, 1998.

Yu, J., Cocker III, D., Griffin, R. J., and Flagan, R. C.: Gas-Phase Ozone Oxidation of Monoterpenes: Gaseous and Particulate Products, 207–258, https://doi.org/10.1023/A, 1999.

Zeng, T., Wang, Y., Yoshida, Y., Tian, D., Russell, A. G., and Barnard, W. R.: Impacts of prescribed fires on air quality over the Southeastern United States in spring based on modeling and ground/satellite measurements, 42, 8401–8406, https://doi.org/10.1021/es800363d, 2008.

Zhang, H., Yee, L. D., Lee, B. H., Curtis, M. P., Worton, D. R., Isaacman-VanWertz, G., Offenberg, J. H., Lewandowski, M., Kleindienst, T. E., Beaver, M. R., Holder, A. L., Lonneman, W. A., Docherty, K. S., Jaoui, M., Pye, H. O. T., Hu, W., Day, D. A., Campuzano-Jost, P., Jimenez, J. L., Guo, H., Weber, R. J., de Gouw, J., Koss, A. R., Edgerton, E. S., Brune, W., Mohr, C., Lopez-Hilfiker, F. D., Lutz, A., Kreisberg, N. M., Spielman, S. R., Hering, S. V., Wilson, K. R., Thornton, J. A., and Goldstein, A. H.: Monoterpenes are the largest source of summertime organic aerosol in the southeastern United States, Proc Natl Acad Sci USA, 115, 2038–2043, https://doi.org/10.1073/pnas.1717513115, 2018.

Zhang, X., Hecobian, A., Zheng, M., Frank, N. H., and Weber, R. J.: Biomass burning impact on PM2.5 over the southeastern US during 2007: Integrating chemically speciated FRM filter measurements, MODIS fire counts and PMF analysis, 10, 6839–6853, https://doi.org/10.5194/acp-10-6839-2010, 2010.

Zhang, Y. and Wang, Y.: Climate-driven ground-level ozone extreme in the fall over the Southeast United States, Proc Natl Acad Sci USA, 113, 10025–10030, https://doi.org/10.1073/pnas.1602563113, 2016.

Zheng, Y., Thornton, J. A., Ng, N. L., Cao, H., Henze, D. K., McDuffie, E. E., Hu, W., Jimenez, J. L., Marais, E. A., Edgerton, E., and Mao, J.: Long-term observational constraints of organic aerosol dependence on inorganic species in the southeast US, Aerosols/Atmospheric Modelling/Troposphere/Chemistry (chemical composition and reactions), https://doi.org/10.5194/acp-2020-575, 2020.

Ziemann, P. J. and Atkinson, R.: Kinetics, products, and mechanisms of secondary organic aerosol formation, 41, 6582, https://doi.org/10.1039/c2cs35122f, 2012.